Grant Agreement Number 608553

IMAGE
Integrated Methods for Advanced Geothermal Exploration

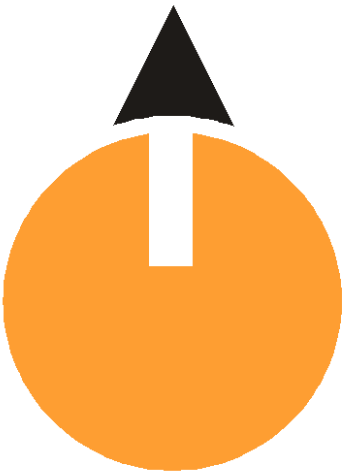

IMAGE-D8.1:
Selection of exploration techniques

Responsible author	C. Dezayes (BRGM)
Responsible WP-leader	C. Dezayes (BRGM)
Contributions by:	Mathieu Darnet Nicolas Coppo Mikael Delatre Chrystel Dezayes Mariane Peter Arnold Blaisonneau,

1 Executive Summary

The field integration workpackage (WP8) is dedicated to integrate all existing and new data derived from new exploration techniques to provide predictive models for site characterization and well-sitting. The objective of this workpackage is to provide a systematic approach for the assessment of an optimum location of geothermal production and injection wells. For that, it aims at provide recommendations to the use of existing and novel exploration techniques developed and tested in the WP7 in order to highlight the favorable key situations identified in the WP6.

Patterns and situations favourable to enable geothermal exploitation can be classified according to the two main factors: heat and fluid flow and accumulation:
- Heat factor: patterns that enable positive heat anomaly, *i.e.* that result in having higher temperature at one given depth than in a classic situation of normal geothermal gradient;
- Fluid factor: patterns that enable fluid flow and that may be favourable to expect final sufficient flow (after enhanced processes) for a viable exploitation.
The most important key situations take into account for the geothermal exploration of deep basin and basement are the presence of a plutonic intrusion, a thermal blancket, a convective transfert system, a fracture pattern like joke, ramp, tip and fracture intersections.

Theorically, these key situations are not scale-dependent but in an exploration context, different scales have to be considered: the European scale, the regional scale and the local scale. The size of geological objects considered for each scale is curcial for the selection of the exploration methods. A synthesis of the exploration methods versus key situations at the different scale is provided in this report. There are therefore no golden rules to select the best exploration techniques for a given geothermal project in a sedimentary basin but rather a wealth of techniques that must be tailored based on their technical feasibility, spatial resolution, delivery time and costs.

Table of Content

2 Introduction

The field integration work package (WP8) is dedicated to integrate all existing and new data derived from new exploration techniques to provide predictive models for site characterization and well-sitting. The objective of this work package is to provide a systematic approach for the assessment of an optimum location of geothermal production and injection wells. For that, it aims at provide recommendations to the use of existing and novel exploration techniques developed and tested in the WP7 in order to highlight the favorable key situations identified in the WP6.

This report is the first deliverable of the field integration work package. In the first section, the key situations, key parameters and different scales of the geothermal targets are summarized in order to define which geological objects have to be characterized. Then, a summary of the different methods (i.e. geophysics, geology, geochemistry) are presented including their principle, benefits, resolution and limitations. The different types and the different scales of the thermal and/or hydromechanical models are also presented to give a basis of the building of local predictive models that will be performed in the next task of the work package. Taking all of the above into account, we finally provide some guidance as to which techniques are potentially the most appropriate to optimize the drilling location of the future wells to ensure best flow performance and temperature.

3 Key Situations for Deep Geothermal Reservoir Development in Sedimentary Basins

3.1 Introduction

The widespread exploitation of the in-depth heat by EGS (Engineered Geothermal System) techniques requires re-thinking the approaches to move towards an optimized and adapted exploration designed to minimize the "geological" risk. The present-day prospected resources correspond often to deep hydraulic systems more or less continuous, heterogeneous and localized; globally, they show no real geothermal manifestations at surface. In this context, the difficulty is then to identify the most favourable areas before any significant capital investment. In these specific contexts, favourable areas cover the prospected temperature depending on the final use and the initial hydraulic potential to minimize the subsequent potential risks due to the enhancement of the injection/production flow rate of the exploitation wells.
In recent years, the ongoing work on the EGS and on the characterization of the associated potential resource leads us to try to define "key situations". The goal of these "key situations" is to try to understand how they allow an initial discrimination during the exploration phase to choose the location of the first exploratory drillings. In this context, key situations could be defined as patterns that suggest that there is a resource having sufficient temperature and flow at an economically viable depth (optimization of the depth to reduce the drilling cost). The understanding of the key situations and their interaction will help to develop guides for exploration methodology and in particular should constraint the exploration methods as geophysical measurements, by defining objects that have to be identified (constraint on the method) and their size (resolution constraint).
Patterns and situations favourable to enable geothermal exploitation can be classified according to the two main factors: heat and fluid flow and accumulation:
- Heat factor: patterns that enable positive heat anomaly, *i.e.* that result in having higher temperature at one given depth than in a classic situation of normal geothermal gradient;
- Fluid factor: patterns that enable fluid flow and that may be favourable to expect final sufficient flow (after enhanced processes) for a viable exploitation.

3.2 Key Situations and Corresponding Conceptual Models

3.2.1 Heat factor

During the exploration phase, an initial discrimination must focus on a resource having sufficient temperature at an economically viable depth. The heat elementary key situations are patterns that suggest a positive heat anomaly. Three main patterns can be encountered (Figure 1):

- Intruding rock - Heat anomaly is due to the radioactive decay of elements in an intruding rock. (Richardson & Oxburgh, 1979)
- Thermal blanket - Due to their high porosities, the thermally low-conductive sediments acts as a thermal blanket, causing heat storage in the basin. The blanketing effect of sedimentation on crustal heat flow is largest for high sedimentation rates and sediments with low thermal conductivities. Heat anomaly amplitude depends on the rock nature, the rock mass structure, and associated properties (thermal conductivity), the thickness of the blanket and its shape. (Cacace , 2010, Theissen and Rüpke, 2009, Van Wees , 2009).
- Convective heat transfer - Convection cells (liquids, gaz…) happens when the warmer and less dense fluid rises while the cooler fluid drops down. It results in homogenizing the temperature profile (no gradient of temperature). The heat anomaly amplitude depends on the physical situation that enables the fluid motion, and of the fluid properties

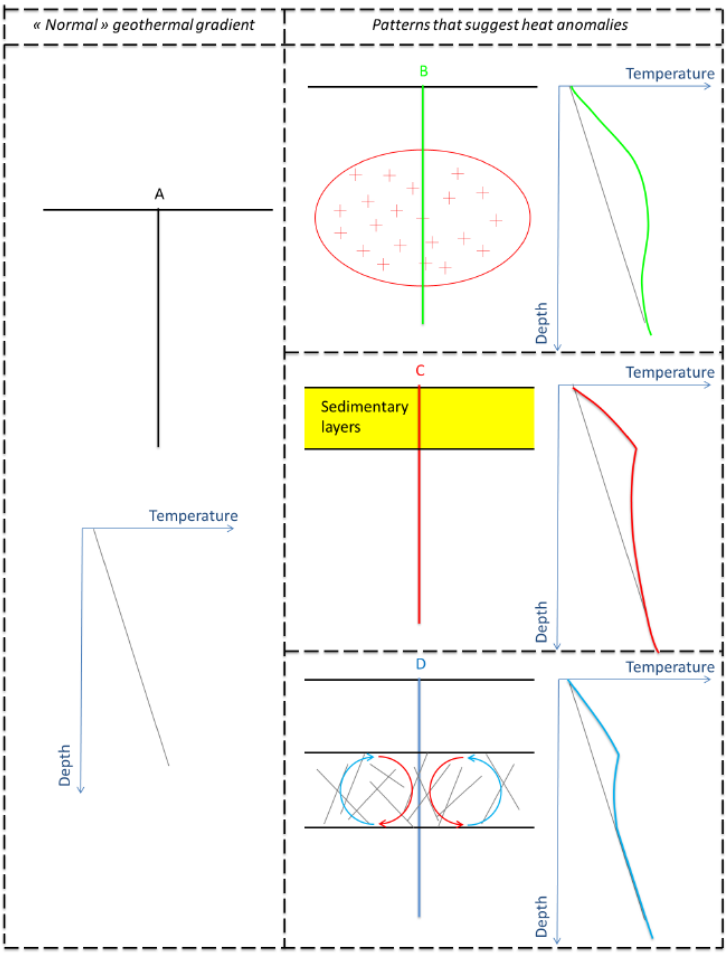

Figure 1: Patterns that enable positive heat anomaly compared to a normal geothermal gradient (A). B. – Plutonic intrusion (heat production due to radioactive decay). C. – Thermal blanket. D. – Convective heat transfer (the pattern enabling the fluid circulation is here represented by highly fractured rock mass)

3.2.2 Fluid factor

The fluid flow mainly depends on the bulk permeability of a rock mass that is the result of three main components:
- 1/ the intrinsic permeability of the lithologic units,
- 2/ the anisotropy inherited from rock layering and existing fracture sets; and
- 3/ live structural components affecting the permeability, including faults, fractures and dikes.

The “fluid flow” situations list the different patterns linked to these components and that may be favour a final flow (after enhanced processes) sufficient enough for a viable exploitation. Faults specific features and local stress states enabling the setup of favourable structures are listed below:

- Within a single fault:
  - Jogs: The formation of jog is associated with new structures creation both normal and strike-slip (dilational or contractional jogs depending if releasing or contractional movement - sktech A. B. D below). Axial flow is further enhanced by the common intersection of stress-controlled brittle structures in jogs. In particular, dilational jogs constitute reservoir as they localize the minimum of stress, and fluid flow at the junction of the lateral margin and the jog-defining fault (Faulds , 2011, Zhang 2015, Zhang , 2007, Sibson, 2000, Connolly & Cosgrove, 1999, Rowland & Sibson, 2004, Micarelli & Benedicto, 2008).

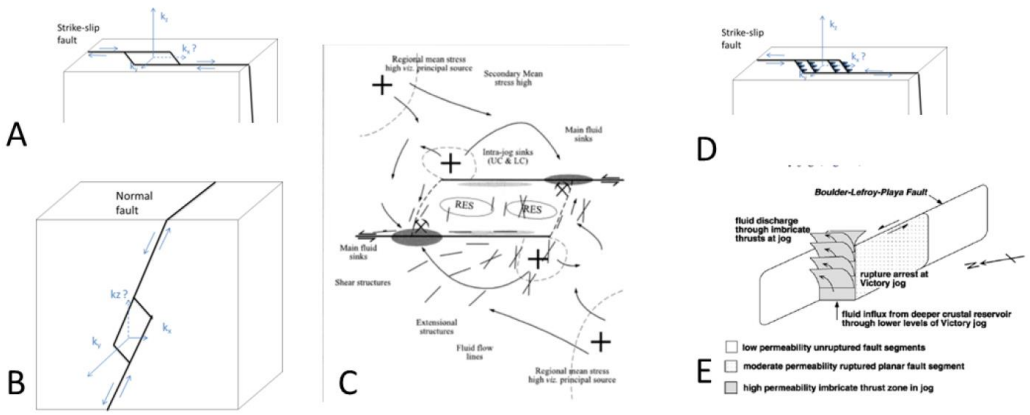

Sketch of jog structures. A : Dilational jog within strike-slip fault. B. Dilational jog within normal fault. C. In detail, fluid accumulation (RES) and flow (ß) areas in 2D in dilational jog. (Connelly and Cosgrove, 1999). D. Contractional jog in strike-slip fault. E. Permeability distribution in contractional jog from Cox & Ruming (2004).

  - Relay ramp: Displacement variation along normal faults is common and the presence of a displacement gradient requires that either one or both of the hanging wall and footwall cutoff lines must differ in length from their original, pre-faulting, lengths. Relay ramp are typically areas where along-strike displacement gradients induce fracturing in footwalls and hanging walls. Induced fractures in the relay ramp areas focus flow in the vertical the direction (as fracture/fault intersections). Relay ramps in extensional fault systems are recognized as zones of localized high strain, related to the large displacement gradients on the bounding faults (Rowland & Sibson, 2004, Ferril & Morris, 2001).

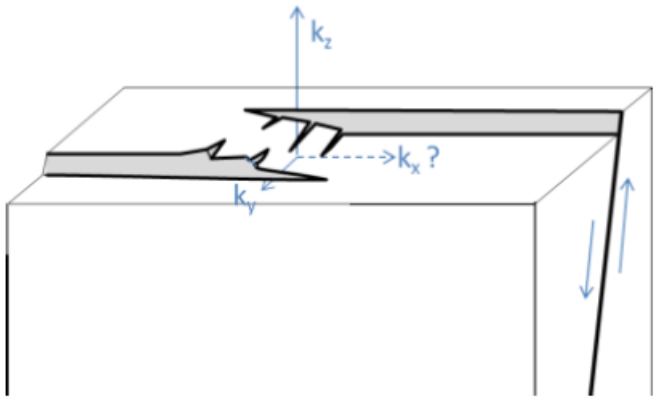

Sketch of enhanced permeability in the relay-ramp area

- Fault tips: Fault tip focus vertical flow, because displacement gradients are typically steeper near fault terminations (tips) than on the fault as a whole. A damaged zone is often associated with fault tip, where wing cracks (B), horsetail fractures(A), antithetic faults, and synthetic branch faults generates a broad area of highly fractured rock.

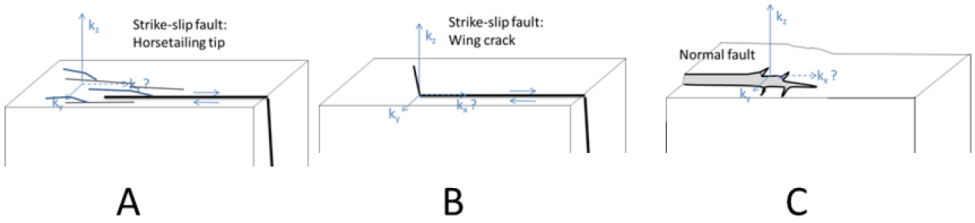

Sketch of enhanced permeability at fault tips – A. Horsetailling tip – B. Wing crack tip – C. Normal fault tip.

- **Faults interaction/intersection zones**
  Fault interaction/intersection zone are located where two or more fault tip-lines are in close proximity (interaction) or intersect (intersection). The individual breakdown regions merge, forming a single, modified breakdown region where stresses associated with the two fault tips interact.
  Faults interaction/intersection focus flow in the direction of the intersection line. Here, stress concentrations cause continual re-opening of fluid-flow conduits, permitting long-lived hydrothermal flow despite potential clogging of fractures due to mineral precipitation (Faulds , 2011, Rowland & Sibson, 2004, Zhang 2015).

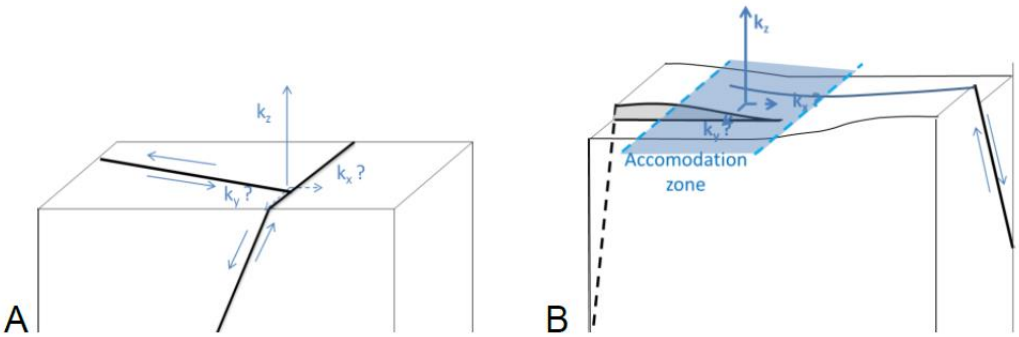

Sketch of enhanced permeability at fault intersections – A. Permeability is enhanced in the direction of the intersection line – B. Example of intersection of two opposite dipping faults (conjugate normal faults): the area that accommodate the displacement constitute a major axis for flow.

3.2.3 Conceptual model

From the previously defined patterns that favour fluid flow, conceptual model has been proposed in a segmented magmatic rift system (Figure 2, Rowland & Sibson 2004). Fluid flow mainly horizontally in rift segment, and variation in faults motion, that are accommodated by different kind of irregularity (as relay ramp, accommodation zones s.s….), favour vertical flow. In rift segment most favourable situations (key situation) for hot fluid vertical flow are then mainly accommodation zones.

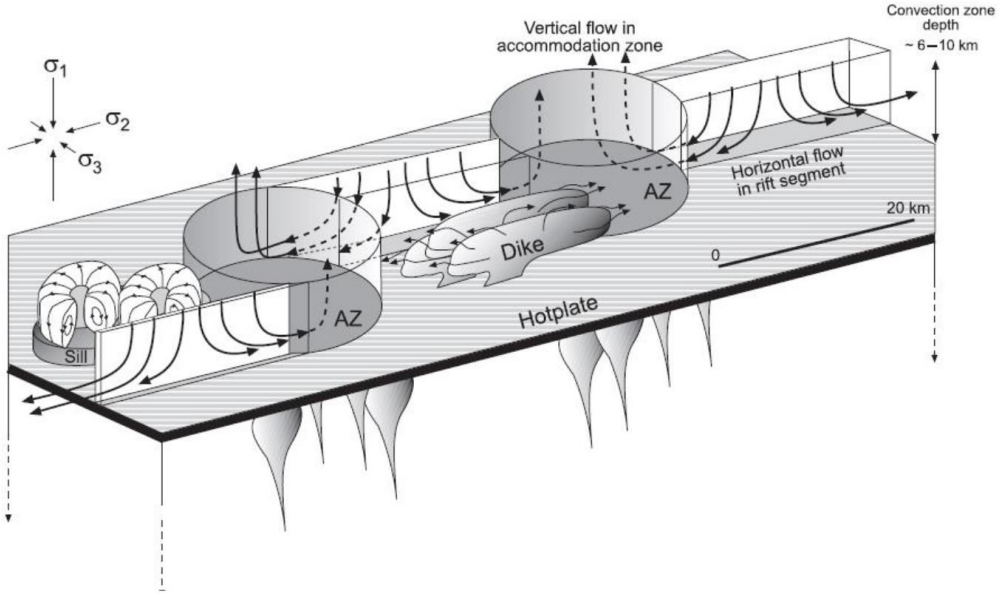

Figure 2: Conceptual model for structurally influenced hydrothermal flow in a segmented magmatic rift model. Heat transfer may be by dike, sill and/or small pluton emplacement, all of which are affected by rift kinematics ; and/or via a large scale hot-plate which is essentially unaffected by rifting. Fluid flow in rift segments is characterized by axial horizontal flow toward accommodation zones, except where sills form localized hot plates. In contrast geothermal plumes preferentially develop in accommodation zones which are region of enhanced vertical permeability (Rowland & Sibson 2004).

3.3 Scale definitions

The key situations presented above can exist at the all scales. However, the selection of exploration methods depends on the scale considered. We will focus here on the scales associated to the different types of models (Figure 3):

- The “European scale” covers every scale from a 1000 km X 1000 km square at the scale of the lithospheric plate. At this scale, the objective is to consider the global stress fields or temperature fields that will constrain regional models, considering parameters such as thickness of the crust or movement of major geological objects. The size of the typical geological object will be about 10’s km.

- The “Regional scale” means an area with an extension of 50 to 100 km. This covers the studied geological object that is considered as relevant as a first step of exploration, because of some of its characteristics (average geothermal gradient or average heat flow, depth of geological formation…). It also includes the immediate surroundings of this geological object to be able to constrain the regional models that will be built. This scale is adapted to a geodynamic structure such as graben, basin… including their borders and the typical geological object size will be about 1’s km.

- The “Local scale” corresponds to scale required at the last step of exploration (i.e. before drilling), when an area of interest has to be chosen for its geothermal potential and location of the first exploration well has to be proposed. The typical extension associated to this scale can be 10 to 30 km and the size of geological object is about 100’s m.
- The “Field scale” corresponds to the licence scale, namely an area of about 1 km X 1 km or less. At this scale, exploration and/or exploitation boreholes will be drilled. At this scale, the typical object size is about 1’s m.
- The “Well scale” corresponds to the area around the well, at about 1 m behind the borehole wall. This scale is necessary to characterize the near-well reservoir behaviour. The typical geological size at this scale is from 1 mm to 1 m.

In the framework of the exploration phase of a geothermal project, therefore in the IMAGE project, we address the three first scales through a systematic workflow approach.

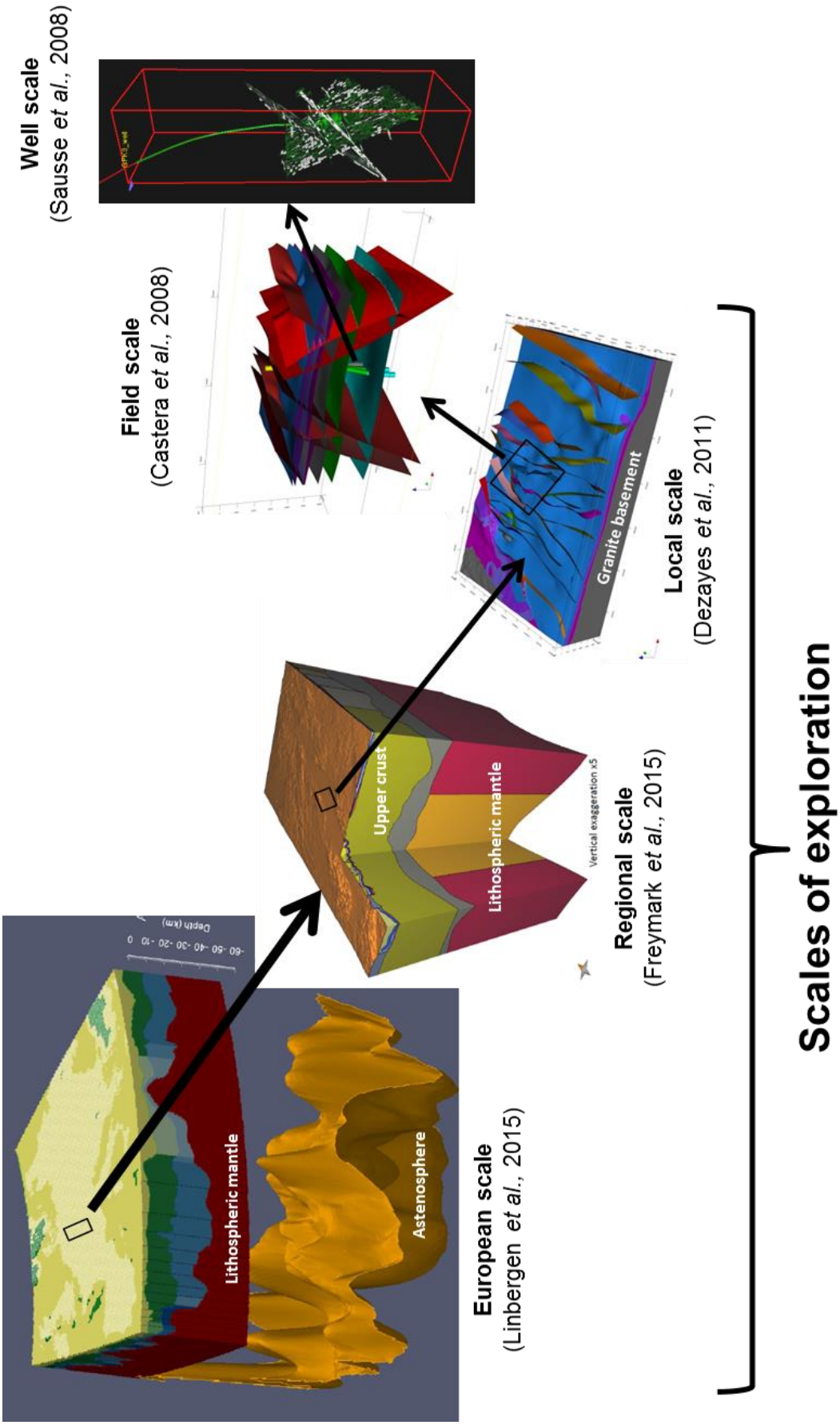

Figure 3 : Illustration of the different scales

3.4 Petrophysical properties of key situations

The selection of geophysical techniques to assess the different key parameters of an exploration area depends very much on the expected contrasts of petro-physical properties in the key situation. In this section, we will therefore give first an overview of a conceptual fault zone model expected in a deep sedimentary basin and describe the expected petro-physical changes. We will then give a few rules of thumbs with respect to the dependency of geophysical observables (resistivity, density and velocity) of a brine-saturated rock on these petro-physical changes.

3.4.1 Conceptual model of a fault zone

Fault zones are complex geological structures and numerous literature are devoted to their study (for example: Caine *et al.*, 1996; Faulkner *et al.*, 2010; Bense *et al.*, 2013; …). Based on the Soultz wells analysis, a conceptual model of fault zone has been built in the hercynian granite basement of the Upper Rhine Graben (Genter *et al.*, 2000).

Fracture zones are organized with a core of intense fracturing in which breccia, microbreccia and cataclasites developed, corresponding to successive stages of brittle deformation (Figure 4). The primary minerals of the granite have been partly dissolved developing a peripheral wall-rock alteration halo. Then, silica-rich fluids precipitated quartz in the inner part of the fracture zone evidenced by the deposition of thicker veins. Surrounding the core in an intermediate zone in which fracturing is less intense. Cataclased granite is present in this zone and hydrothermal alteration is less intense than in the central part. Lastly, an outer zone is characterized by low fracture density but fairly intense argilization of the granite. This outer zone is considered as altered wallrock.

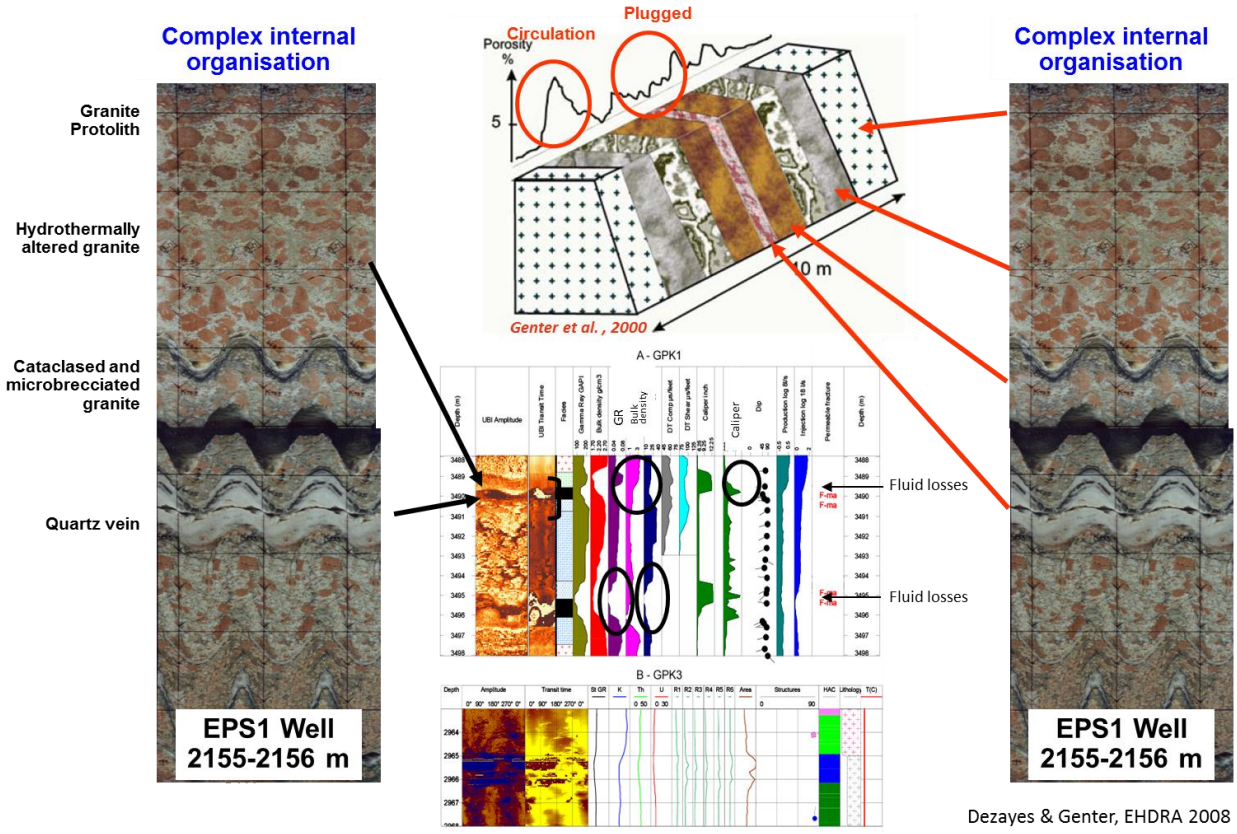

Figure 4: Conceptual model of fault zone derived from the analysis of the faults observed in the Soultz-Sous-Forêts geothermal field.

The porosity of the fresh Soultz granite is less than 1%. Porosity values obtained on whole rock altered samples range between 1.7% and 25%. The fractured-altered samples (breccia, microbreccia) are quite often less porous than the hydrothermally altered facies. This observation is explained if we consider that the macroscopic fractures developed into the breccia facies are systematically sealed by hydrothermal products. These secondary deposits plugged both the fractures and its surrounding altered matrix and then reduced the porosity values. Within the altered facies, the dissolution processes into primary plagioclases and biotites are quite abundant and the porosity values are higher. This is illustrated on Figure 4, which shows that the highest porosity values take place laterally and the lowest values are more or less concentrated into the inner part of the fractured zone. In this inner part, the gammay ray is very low, indicating presence of silica minerals, whereas in the lateral part, this value is high, showing presence of minerals of alteration, such as illite.

3.4.2 Resistivity

The resistivity of a rock depends on three key parameters: the fluid conductivity, the shape and size of the porous network and the conduction phenomena occurring at the mineral interface due to the presence of alteration products. We used the model of Revil and Glover (1998) to describe the dependency of the rock resistivity on the fluid salinity, porosity of the rock, ability of alteration minerals to conduct current (or Cationic Exchange Capacity or CEC) and temperature.

3.4.2.1 Brine Salinity

The higher the salinity, the lower the brine resistivity is as the larger the number of charge carriers is (Figure 5). On the other hand, the higher the temperature, the lower the resistivity of the brine is, as the more mobile the charge carriers are.

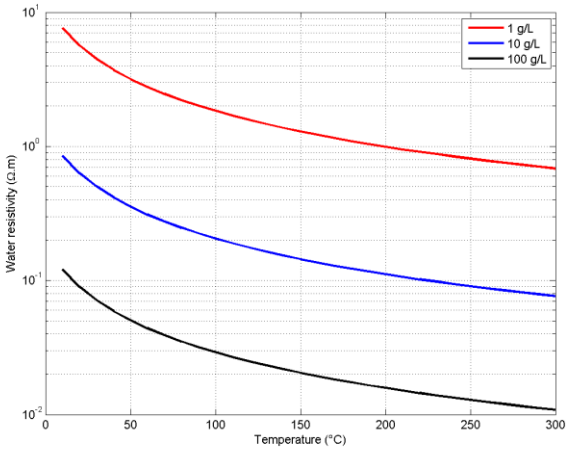

Figure 5: Brine resistivity as a function of temperature and salinity.

3.4.2.2 Rock resistivity

For a rock free of alteration minerals, the higher the temperature, the lower the rock resistivity is (Figure 6). Similarly, the higher the brine salinity, the lower the rock resistivity is and the higher the porosity, the lower the rock resistivity is. The dependencies all express the ability of the rock to conduct electrical current through the fluid filling the porous network.

For a rock with alteration minerals, the conduction of electric current through the fluid filling the pore space is offset by the conduction through the alteration minerals. Indeed, the higher the CEC, the lower the rock resistivity is but also the weaker the influence of the brine salinity is (Figure 7).
For a fault zone with an alteration zone showing an increased porosity and filled with hot geothermal brine and where alteration minerals are present, the conduction of electrical current through the brine in the pore space and alteration minerals are both going to decrease significantly the resistivity of rock (in our simplified model, resistivity is going to drop by several orders of magnitude). Such a drop of resistivity has been observed in actual well logs (Figure 8) and confirms the expected large variation of resistivity in a fault zone.

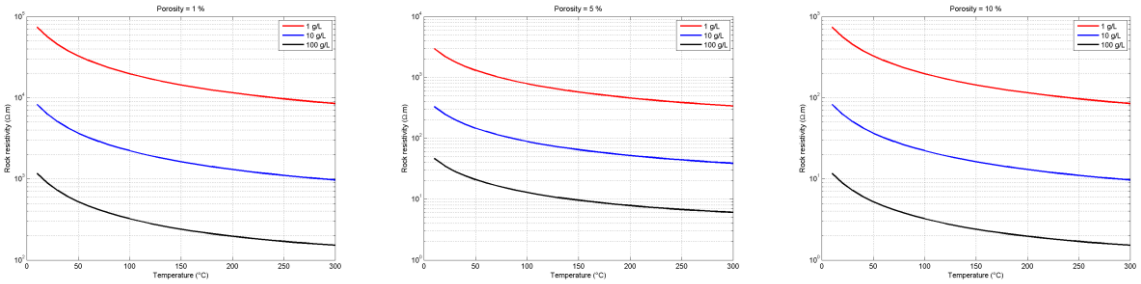

Figure 6: Resistivity of a rock free of alteration minerals as function of temperature and brine salinity from left to right for a 1%, 5% and 10% porosity.

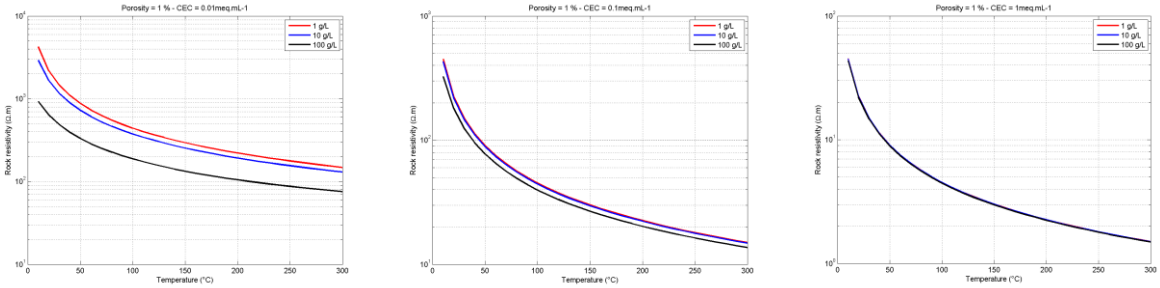

Figure 7: Resistivity of a 1% porosity rock with alteration minerals with increasing cationic exchange capacity (from left to right from 0.01 to 0.1 and 1 meq/mL) as function of temperature and brine salinity.

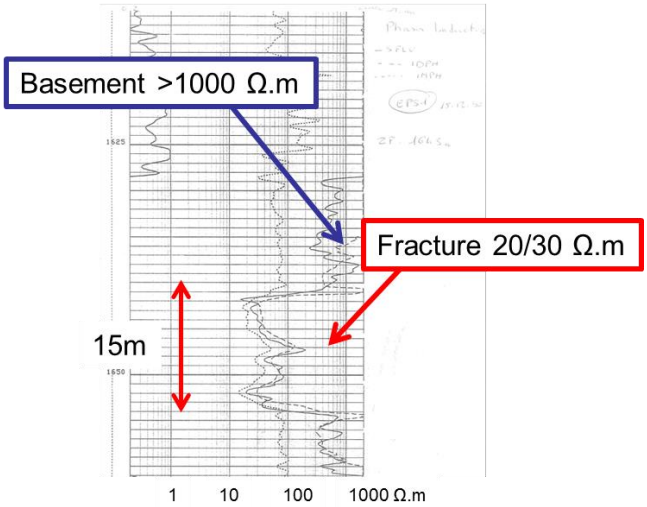

Figure 8: Resistivity log through a fault zone in the Soult-sous-Forêts geothermal field.

3.4.3 Density

3.4.3.1 Brine density

The temperature dependence of a brine under 1 atmosphere is given on Figure 9 (Batzle and Wang, 1992). The higher the temperature, the lower the density is but the higher salinity, the higher the density is. Similarly the higher the confining pressure, the lower the density is (Figure 10) but the influence is much less than the temperature.

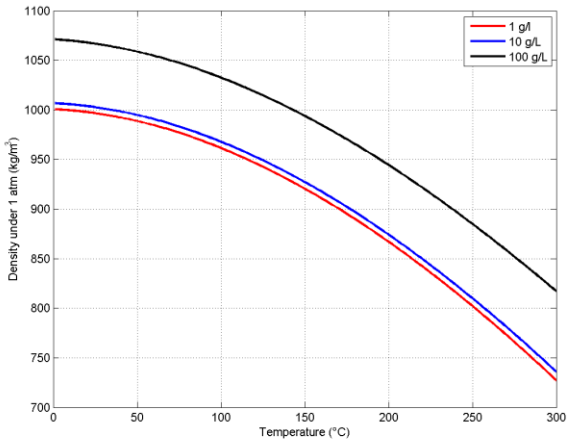

Figure 9: Brine density as a function of temperature and salinity.

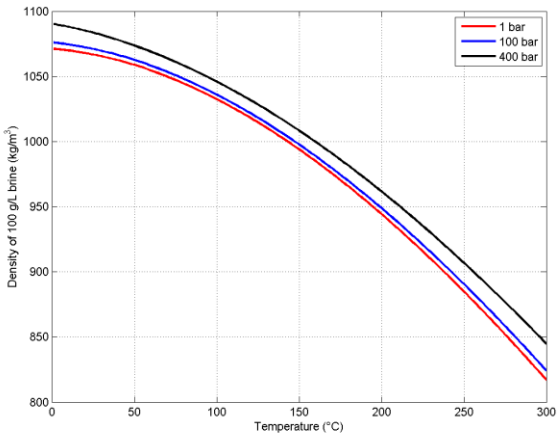

Figure 10: Brine density of 100 g/L of NaCl as a function of temperature and confining pressure.

3.4.3.2 Rock density

The temperature dependence of the density of granitic rock filled with 100 g/L NaCl brine at 400bar is given on Figure 11, assuming a density of 2800 kg/m3 for unaltered granite. It clearly shows that the density of granite is a lot more sensitive to porosity variations than temperature.

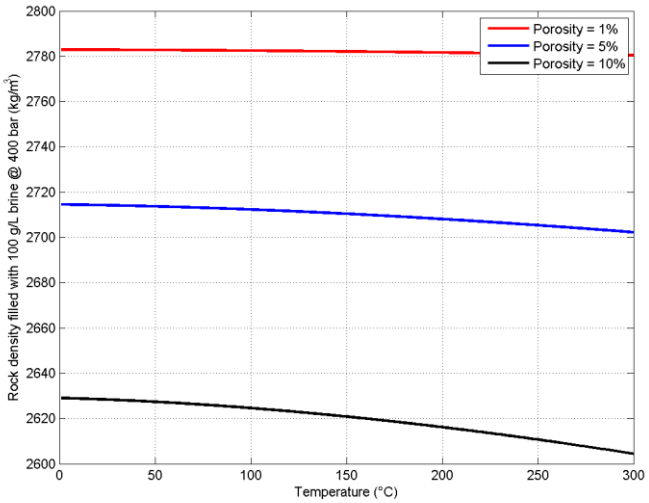

Figure 11: Granite density filled with a 100 g/L NaCl brine as a function of temperature and porosity.

3.4.4 Seismic velocity

3.4.4.1 Brine velocity

The temperature dependence of the velocity of 100 g/L brine has been calculated using Batzle and Wang (1992) formulas (Figure 12). The higher the temperature, the lower the velocity is (due to the drop of bulk modulus with temperature).

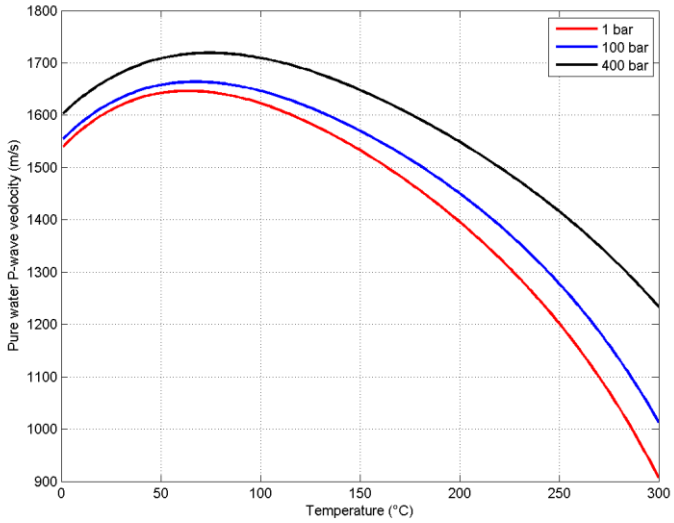

Figure 12: 100 g/L brine compressional velocity as function of temperature and pressure.

3.4.4.2 Rock velocity

The temperature and pressure dependence of the P and S-wave velocities of a rock is difficult to predict in a general case as it requires knowing the temperature and pressure dependence of the bulk and shearing moduli of the minerals and of the dry rock. In general, the P-wave and S-wave velocity of a granite increase with increasing effective pressure (Figure 13). On the other hand, P and S-wave of a granite usually decrease with increasing temperature (Figure 14).
Similarly to the rock density, the overriding factor for rocks sitting in deep sedimentary basins is likely to be the porosity and/or degree of alteration encountered. An example taken from the Soults-sous-Forêts granite nicely illustrates that the main parameter affecting P and S-wave velocities is the density of fractures (Figure 15).

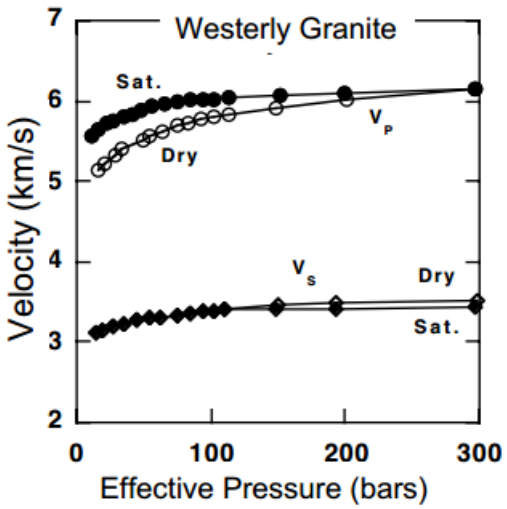

Figure 13: P and S-wave velocity dependence of a granite on effective stress at constant temperature.

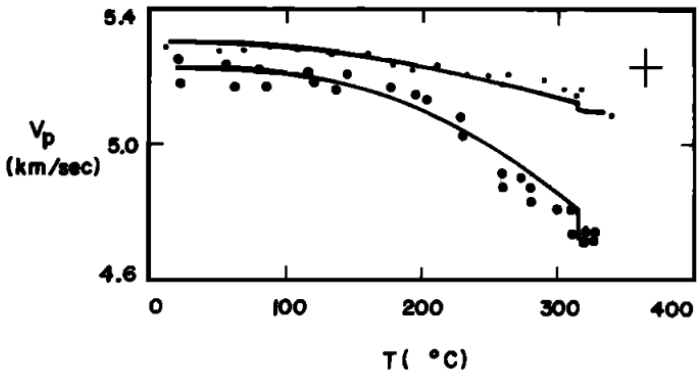

Figure 14: P and S-wave velocity dependence of two granites on temperature at constant effective stress (Spencer and Mur, 1976).

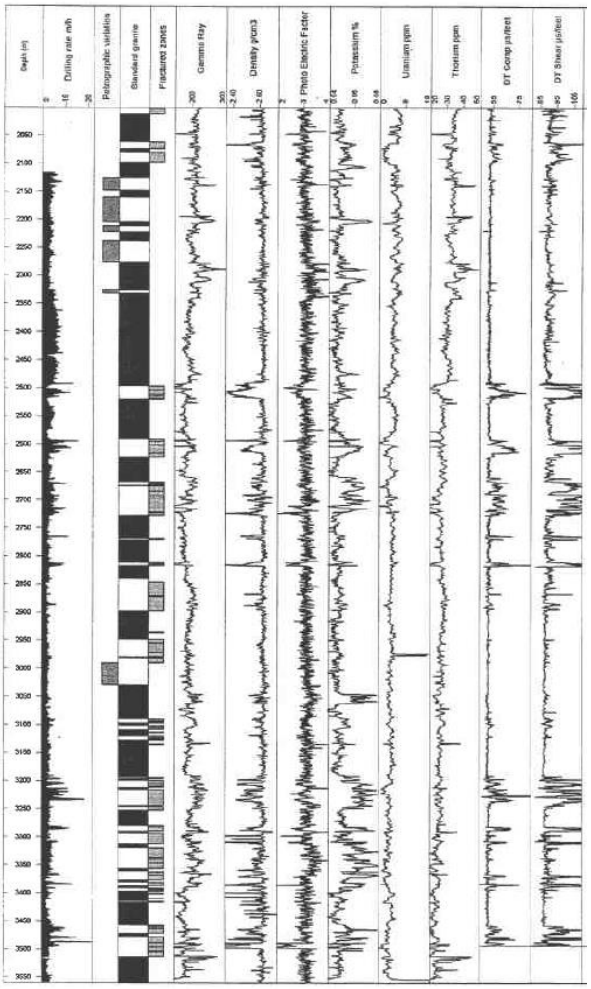

Figure 15: Geological and well logging through the Soultz-sous-Forêts GPK1 well (Genter et al., 1997).

4 Geophysical methods for deep geothermal exploration

4.1 Active seismic

4.1.1 2D/3D Reflection seismic

4.1.1.1 Principle

The reflection seismic technique refers to the technique to measure and display the three-dimensional distribution of velocity or reflectivity of a volume of the Earth by using numerous sources and receivers at the Earth's surface. A 3D seismic reflection survey consists in a set of numerous closely-spaced seismic lines that provide a high spatially sampled measure of subsurface reflectivity. Typical receiver line spacing can range from 300 m to over 600 m, and typical distances between shotpoints and receiver groups is 25 m. Bin sizes are commonly 25 m. The resultant data set can be "cut" in any direction but still display a well sampled seismic section. The original seismic lines are called in-lines. Lines displayed perpendicular to in-lines are called crosslines. In a properly migrated 3D seismic data set, events are placed in their proper vertical and horizontal positions, providing more accurate subsurface maps than can be constructed on the basis of more widely spaced 2D seismic lines, between which significant interpolation might be necessary. In particular, 3D seismic data provide detailed information about fault distribution and subsurface structures. Computer-based interpretation and display of 3D seismic data allow for more thorough analysis than 2D seismic data.
More details on the state-of-the art seismic techniques can be found in the IMAGE milestone report (Greenhalgh et al. 2015).

4.1.1.2 Benefits

The main advantage of seismic reflection techniques is its ability to map subsurface structures over a large area (much larger than what well information can provide). Indeed, any contrast of density and/or acoustic velocity (greater than the first Fresnel zone) will bounce seismic energy back at the geophones. Migrating these reflections back at the reflection points allows constructing an image of the contrasts of acoustic impedance (velocity times velocity) at depth. For geothermal exploration in sedimentary basins, it therefore provides the great advantage of being able to map offsets between different faults blocks (Figure 16) and hence image the fault framework at the target depth (in 2D see Figure 17 and 3D see Figure 18).

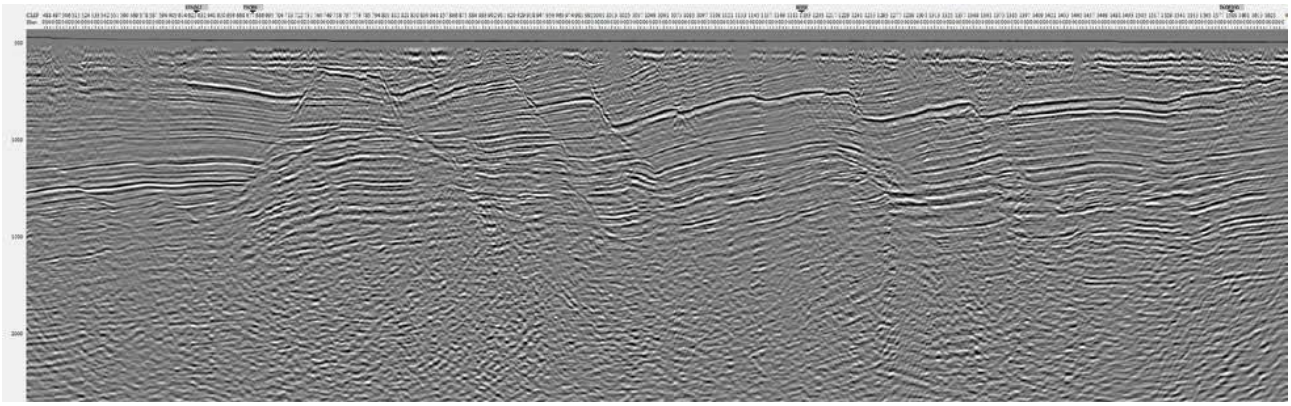

Figure 16: Example seismic reflectivity cross-section obtained from 2D seismic line in the Rhine graben. Please note the different offsets between the seismic reflectors highlighting the main faults of the area (BRGM report, rp 60387).

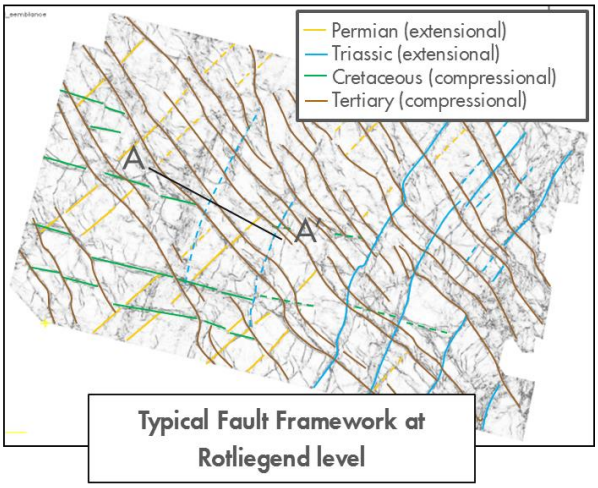

Figure 17: Example of fault framework inferred from the analysis of 3D seismic data at the depth of interest for deep geothermal development in a sedimentary basin in the Dutch North Sea

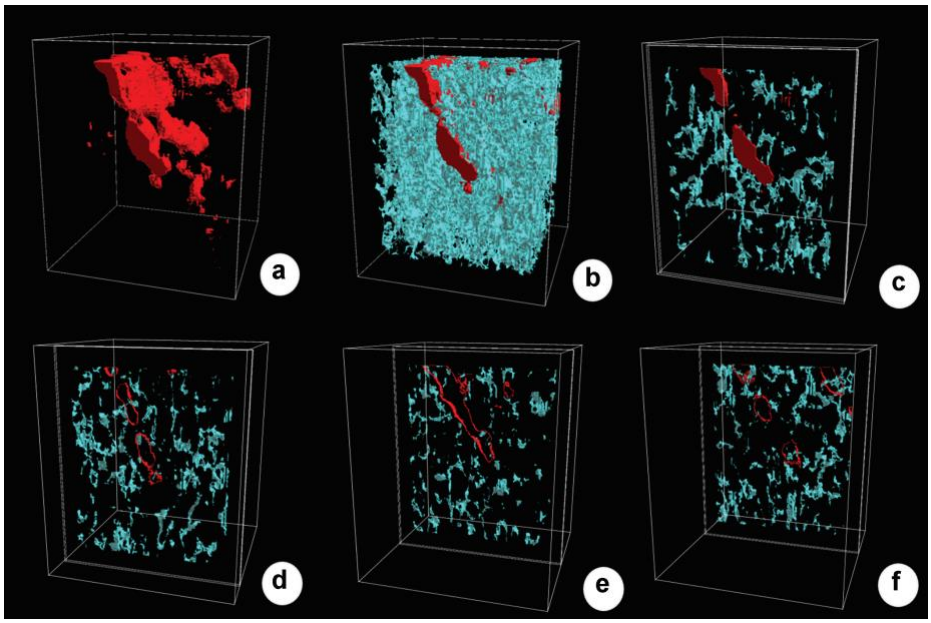

Figure 18: 3D views of large and middle-scale faults and fractures derived from the structural analysis of 3D seismic data over the KTB drill site (Szalaiova et al., 2015). (a) Large-scale faults. (b) Network of all identified large and middle-scale faults and fractures. (c)–(f) Top right and bottom: slices through the volume.

Another advantage resides in analyzing the ratio of amplitude of the reflected wave to the incident wave, or how much energy is reflected. Indeed, variations in seismic reflection amplitude with change in distance between shotpoint and receiver (amplitude versus offset or AVO) indicates differences in lithology and fluid content in rocks above and below the reflector.
For geothermal exploration in sedimentary basins, it can be used to provide an indication of the preferred fracture orientations using amplitude versus offset analysis (AVO) or by studying amplitude variations with azimuth (AVAz). An example from from the analysis of azimuth-dependent amplitude variations is shown on Figure 19. This however requires the 3D seismic survey to be designed to acquire wide-azimuth data (WAZ).

Multicomponent seismic experiments offer the advantage of recording polarization information in addition to amplitude and phase information. This enables the examination of P-, S-, and mode-

converted waves and hence extends the imaging possibilities. Shear waves split into fast and slow modes in anisotropic media such as a fractured reservoir and such birefringence can be used to diagnose and quantify the fracture pattern. Since the propagation of S waves is likely to be sensitive to the fracture orientation, the S wave can be used to determine the fracture orientation.

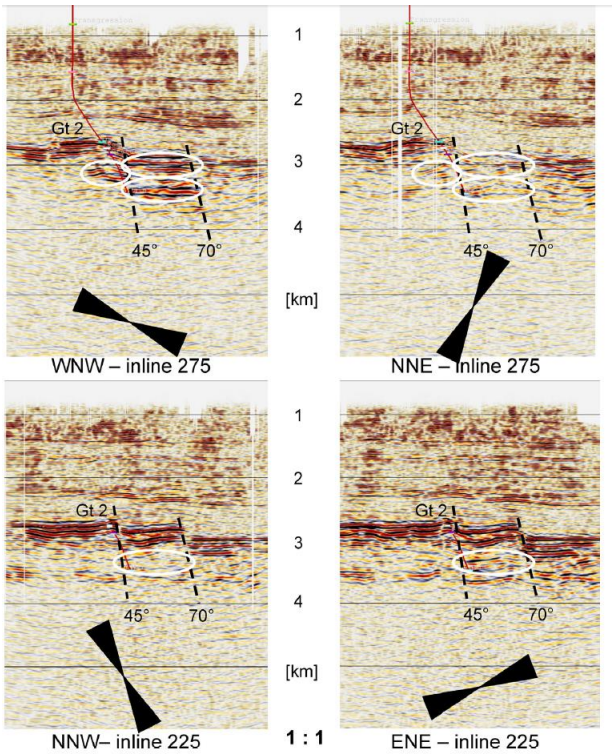

Figure 19: Four vertical sections with different azimuths taken from Lüschen et al. (2014). Dashed black lines mark the main fault zones, red is the trajectory of the borehole and ovals show regions of changing reflectivity for the different azimuths. The amplitudes in the center of the section, close to the Gt 2 well seem to be maximum within the Malm for the ENE azimuth indicating preferred fracture orientation in the same direction.

4.1.1.3 Resolution

Vertical Resolution

Seismic resolution is the ability to distinguish separate features; the minimum distance between 2 features so that the two can be defined separately rather than as one. In order for two nearby reflective interfaces to be distinguished well, they have to be about 1/4 wavelength in thickness (Rayleigh Criterion, Figure 20). For smaller thicknesses than 1/4 wavelength, amplitude correction has to be applied to estimate the bed thickness. For thicknesses larger than 1/4 wavelength we can use the wave shape to estimate the bed thickness.

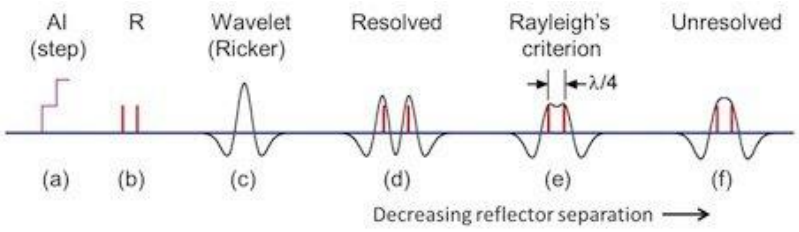

Figure 20: Vertical resolution of seismic waves (Rayleigh criterion)

Assuming the seismic signal has one frequency and that seismic waves travel at one velocity and there is the level of background seismic noise is negligible, the vertical resolution can be written:

$$vertical\ resolution = \frac{\lambda}{4} = \frac{V}{4f}$$

where *V* is the velocity (m/s) and *f* is the peak frequency (Hz). The higher the frequency is, the higher the resolution (Figure 21). There is however a practical limitation in generating high frequencies that can penetrate large depths. Indeed, the earth acts as a natural filter removing the higher frequencies more readily than the lower frequencies as follow:

$$A(t) = A(z = 0)e^{-\frac{\pi f t}{Q}}$$

For weathered sedimentary rocks, Q is around 30 and high frequencies are strongly attenuated with depth (Figure 22). For intact granite, Q is around 1000 and almost no loss of energy occurs. At the depth of geothermal interest in deep sedimentary basins (4/5km), peak frequencies are therefore expected to be in the range of 20/30Hz providing a vertical resolution in order of 30/40 meters.

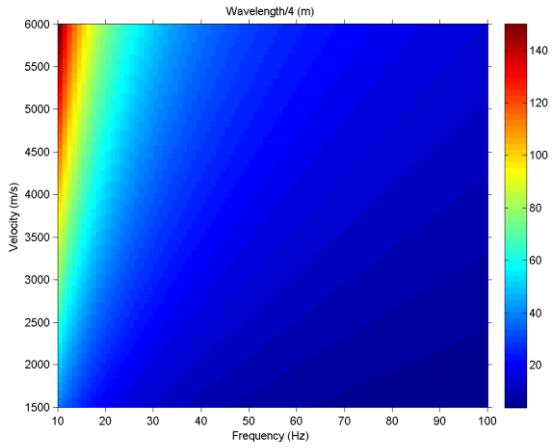

Figure 21: Vertical resolution (in meters) as a function of seismic peak frequency and velocity.

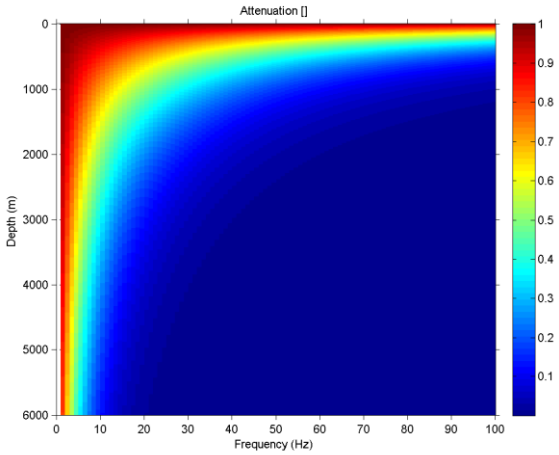

Figure 22: Attenuation factor as a function of seismic peak frequency and depth for sedimentary rocks (Q=30 and Vp = 3000 m/s)

Horizontal resolution

Horizontal resolution refers to how close two reflecting points can be situated horizontally, and yet be recognized as two separate points rather than one. The area that produces the seismic reflection is known as the First Fresnel Zone: the frequency- and range-dependent area of a reflector from which most of the energy of a reflection is returned and arrival times differ by less than half a period from the first break. Waves with such arrival times will interfere constructively and so be detected as a single arrival. Subsurface features smaller than the Fresnel zone usually cannot be detected using seismic waves (source: Schlumberger Oilfield glossary).

The size of the Fresnel zone pre-migration can be calculated to help assess the minimum size feature that can be resolved from seismic data (Figure 23). For sedimentary rocks (Vp ~ 3000 m/s) and at the depth of geothermal interest (depth ~4/5km and hence peak frequency 20/30Hz), the size of the Fresnel zone is around 800m (Figure 24). The migration process fortunately collapses these Fresnel zones (Figure 25), leaving the spatial resolution to be theoretically the same as the temporal resolution (wavelength/4). However, practical limitations such as the aperture of the diffractions or the approximations used in the migration algorithm do reduce the horizontal resolution. For sedimentary rocks and at the depth of geothermal interest, the horizontal resolution is therefore in order of 30/40 meters. As a consequence, 3D seismic data are traditionally processed with bin sizes of 25m but for shallow applications (<1km), high-resolution processing can be applied with smaller bin sizes (e.g. 6.25m).

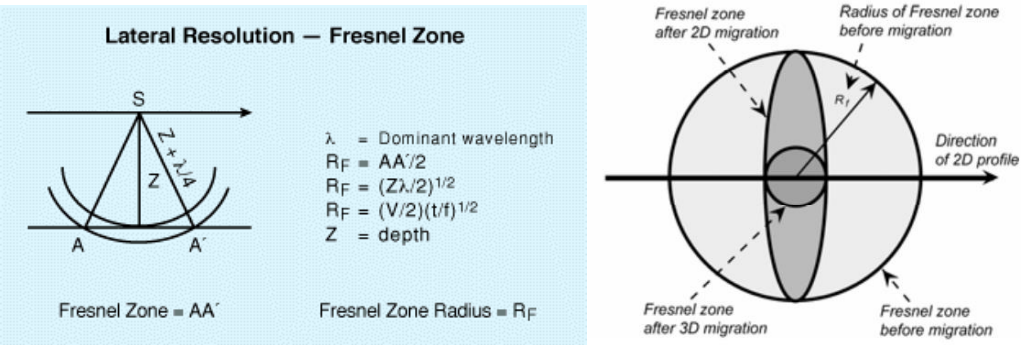

Figure 23: Spherical divergence and attenuation of seismic waves causes a Fresnel zone, shown in this 2D sketch as length A-A'.

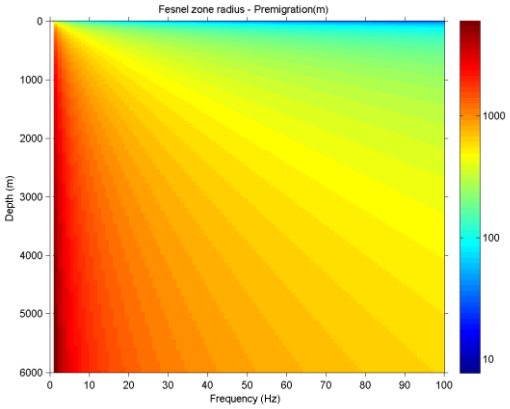

Figure 24: Size of the Fresnel zone pre-migration.

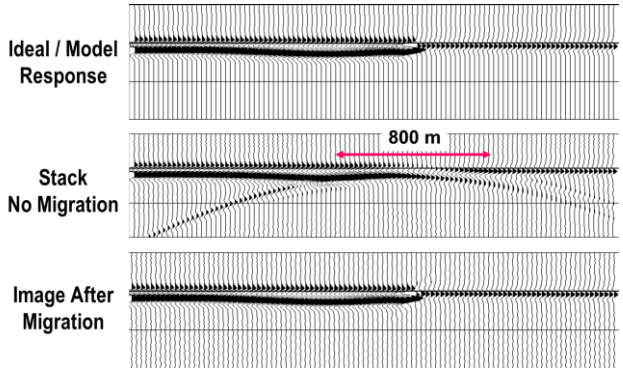

Figure 25: Example of lateral resolution enhancement due to migration (middle: pre-migration, bottom: post-migration)

2D versus 3D seismic acquisition and imaging

2D seismic reflection techniques have proven to be a useful tool for imaging subsurface structures in a variety of scales and investigations. 3D seismic reflection techniques have been used widely in hydrocarbon exploration. Descriptions of shallow 3D seismic reflection surveys on land started to appear in the late 1990s. Recently, there is a trend of substantial reduction in costs related to acquisition and processing of 3D data resulting in small-scale 3D surveys becoming even more common. 2D seismic data are normally used to obtain a regional overview in an area because such data are relatively cheap to acquire, compared to 3D seismic data. However, for more detailed mapping, 3D seismic data are required. The benefit of 3D seismic over conventional 2D seismic includes a dramatic increase in information and accuracy of structural images of the subsurface.

For 2D acquisition, we assume implicitly that the earth is a cylinder, the axis of which is orthogonal to the direction of the survey. However, this assumption is not fulfilled. Thus, interpretation of 2D seismic produces a distorted image. Figure 26 shows the main reasons why 2D seismic interpretation produces distorted images when one is imaging 3D structures. The point diffractor R3d is out-of-the-plane with respect to the 2D acquisition direction. Reflections are incorrectly back-propagated in the earth along the vertical plane passing through the acquisition direction, and are imaged at the wrong location, R2d. To image the diffractor at its correct location, R3d, one must apply 3D imaging for back-propagating the recorded reflection along an oblique plane. However, even after applying 3D imaging methods to a single 2D line, one would be left with the ambiguity of where to place the diffractor along the semicircular curve perpendicular to the acquisition direction, marked as “crossline migration” in Figure 26. For 2D imaging, the error in positioning of the diffractor has both a crossline direction component, Δy and more importantly, a depth component, Δz i.e. geological structures are wrongly positioned in depth. To resolve this ambiguity, one estimates the crossline component of the propagation direction, that is, by recording 3D data.

3D seismic information not only can increase the accuracy of structural images of the subsurface, but can also provide a wealth of stratigraphic information that is not present in 2D seismic data. Horizontal slicing of 3D data volumes facilitates structural interpretations by allowing critical horizons and other features (e.g., faults, channels) to be identified and mapped. Recording data with a wide source-receiver azimuth provides additional information of subsurface targets. This additional illumination may be crucial to generation of interpretable images where targets lie under complex overburden.

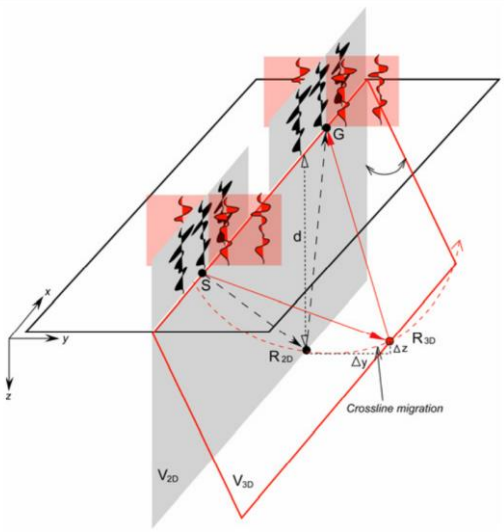

Figure 26: Imaging of an out-of-plane diffractor. In 2D acquisition and imaging, only the in-plane propagation direction can be determined. In 3D acquisition and processing, data contained in the red traces allow unambiguous determination of the propagation direction and position of the diffractor.

4.1.1.4 Limitations

As already described in the previous section, the high-frequency filtering effect of the sediments limits the highest frequency at which seismic waves can be reflected back from deep geothermal targets and therefore limits the vertical and horizontal resolutions to a few tens of meters.

Another key limitation is caused by attenuation due the scattering of the seismic waves. Indeed, whenever there are material changes the energy of a wavefield is scattered in different phases. Depending on the material properties this will lead to amplitude decay and dispersive effects. The parameters governing the kind of scattering are the wavenumber (or wavelength), the correlation length of the scatterers and the propagation distance in the scattering medium. A typical scattering media are magmatic rocks like basalts layers (Figure 27) preventing widespread applications of seismic techniques for geothermal exploration in magmatic areas. A promising alternative might come from the development of broadband vibroseis capable of emitting low-frequency signals (<10Hz) that are less likely to scatter in volcanic rocks (as low-frequency wavelengths are much longer).

Finally, significant limitations arise from the physical constraints in seismic acquisitions e.g. limited access to land (cities, protected areas, lakes etc…), legal limit for seismic source vibrations, high levels of cultural noise. Also, it is important to take into account the fact the seismic acquisition grid (where seismic data is physically being acquired) is much larger than the size of the survey area (that will be properly imaged), usually defined as

$$Acquisition\ grid = Survey\ area + \ Fresnel\ zone + Spread\ Length + Zero\ Offset\ Distance$$

A typical example from Lüschen et al. (2014) is shown on Figure 28 illustrating the various challenges a 3D seismic survey faces in urban areas.

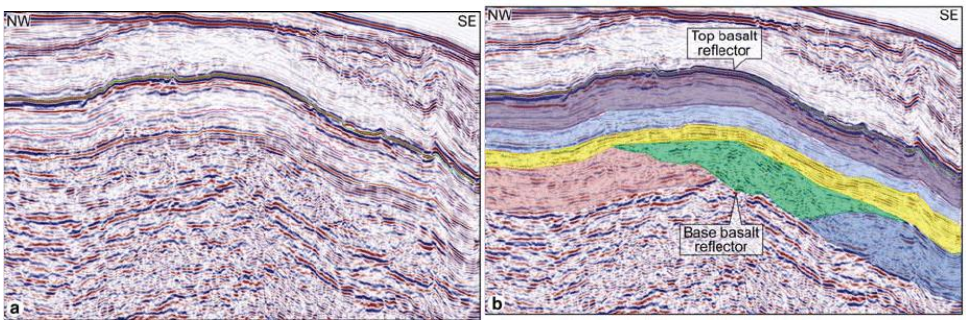

Figure 27: Example of the scattering effect of basalt layers offshore Faroe Islands (Ellefsen et al. 2016). Please note the sharp increase of seismic noise towards the base of the basalt.

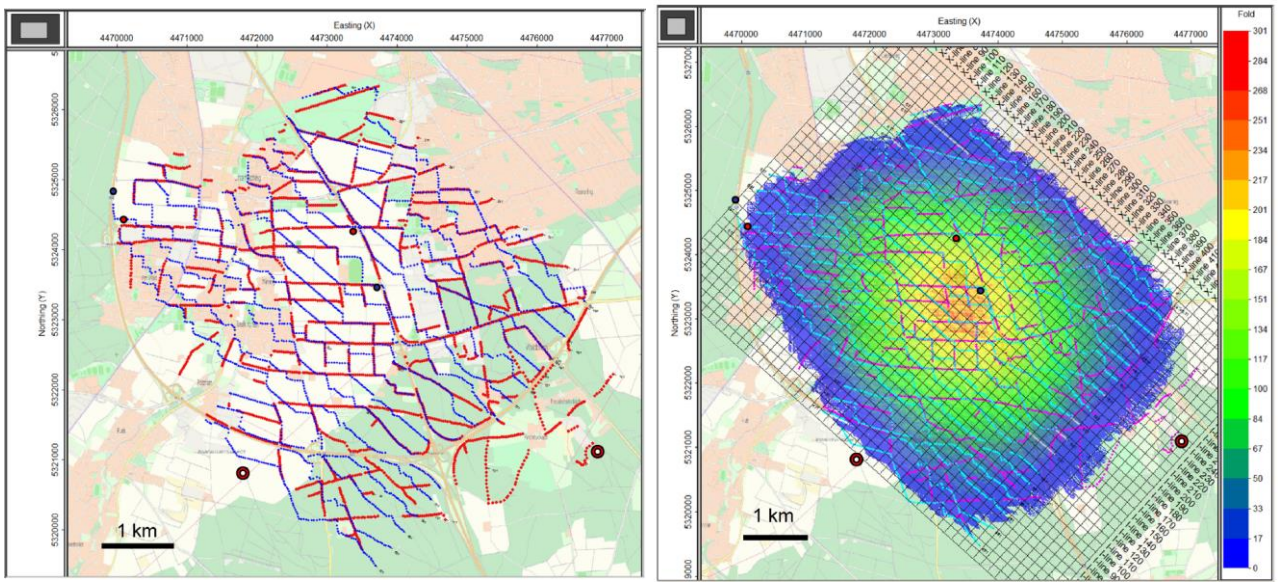

Figure 28: Left: Location map of the 3D seismic survey with vibrator points in red and receiver points in blue color. Rigth: Location map of the 3D seismic survey with bin fold (maximum 301).

4.1.2 VSP

4.1.2.1 Principle

Vertical seismic profiling (VSP) has been widely used to complement surface seismic data. VSP's entail placing receivers downhole and firing into them from surface shots at various offsets (including at wellhead) and azimuths. They can be applied to identify reflections and trace them to their points of origin in the subsurface, provide information about their orientation and exact location when they intersect the borehole, and tie borehole geology to surface seismic data. They provide the elusive link between synthetic seismograms and actual seismic records. Furthermore, they can be used to image structures away from the well.

4.1.2.2 Benefits

There are potentially several advantages of VSP over surface seismic data for deep geothermal exploration:

- Since receivers are placed within the well, travel-times are shorter and therefore the signal amplitudes experience less attenuation than in conventional seismic data. By avoiding traveling twice through the near surface weathered layer, which exhibits high absorption, attenuation is reduced and the higher frequencies preserved for better resolution.
- In order to map dipping features with surface seismic-reflection data, large offsets are required. VSP provides a convenient geometry for mapping gently and steeply dipping interfaces, especially for multi-offset and multi-azimuth surveys.
- Three-component geophones enable the recording of the full vector wavefield and with polarization analysis, the orientation of reflectors can be retrieved, whereas in surface seismic data the polarization information is often lost due to the low velocity near surface layer and the consequent nearly vertically arriving wavefront.

Because of their many advantages, VSP's can be used for high-resolution imaging of lithological interfaces and dipping features in the vicinity of the borehole. Valuable reflectivity, velocity and anisotropy information can be gained from VSP data. Additionally, it is very beneficial for providing a direct linkage between lithology in the borehole and the seismic data, and obtaining accurate velocity values in depth that can be used for the time-depth conversion of surface seismic data.

Place et al. (2010) and Place et al. (2011) investigated the geothermal site in Soultz-sous-Forêts in the upper Rhine Graben with VSP data that was acquired in 1988 and 1993. Diffraction analysis was useful to identify a fault edge and improve the structural interpretation. P-S converted wave analysis indicated steeply dipping fracture zones that control the fluid flow within the granitic basement. A data example indicating different arrivals is shown in Figure 19.

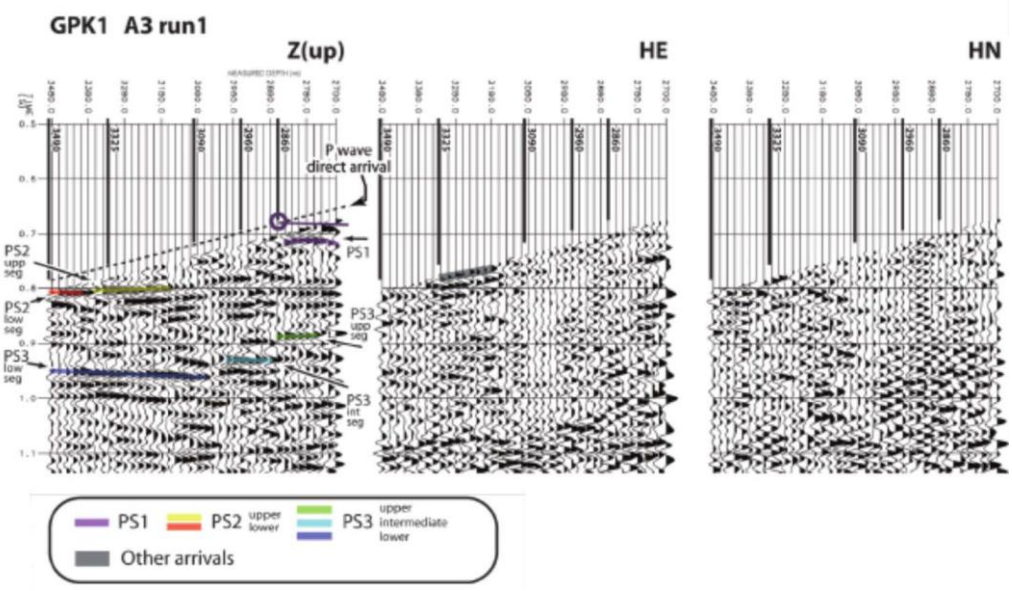

Figure 29*: Three component data from the VSP survey in Soultz-sous-Forêts after isotropic processing taken from Place el. al. (2011). Seismic arrivals are mainly recorded on the vertical component and interpreted as P-S conversion on fault occurring on fault zones.*

4.1.2.3 Resolution

The resolution of the VSP method is similar to the one of the surface reflection seismic method but the smaller number and uneven distribution of receiver and source points reduce significantly the ability of the technique of properly migrating the data away from the borehole and hence its resolution. It is therefore important to perform an illumination study prior to an acquisition in order to define the suitable layout to map the fracture zones of interest.

4.1.2.4 Limitations

The limitations of the VSP technique are similar to the ones of surface seismic reflection (attenuation, scattering, size of the acquisition spread). Additional constraints come from the limited access to the borehole (obstruction zones, presence of geothermal fluids etc…) and limited areal coverage that limits the resolution away from the borehole. It is therefore important to optimize the survey design prior to acquisition (Schmelzbach et al. 2016).

4.2 Passive Seismic

4.2.1 Microseismic Monitoring

4.2.1.1 Principle

Microseismic monitoring aims to detect and locate the seismic events occurring in the studied area during the exploration phase and the exploitation phase. All seismic events are occurring because local stress state can build up over time and generates a movement where it exceeds the least resistant part of the rock, explaining why these events occur preferably along existing faults where weaker parts of the rock can better accommodate the release of stress – thus making these faults active. Active faults can be created ex nihilo provided enough stress is applied to non-fractured rock, but it is far more common that stress buildup is released using pre-existing faults making them “active” (ie with a recorded seismicity), meaning that stress directions and active fault directions may not be perfectly aligned. Seismic events can be complex objects to describe for very large events, for which a rupture is initiated and then propagates with a finite and variable propagation speed for dozens, hundreds or even for thousands of kilometers until the resistance of the rocks is too strong for the diminishing force ; the research is still ongoing to correctly model such mega-events. Fortunately, geothermal exploration usually considers small events for which simple and robust models (Brune 1970) can be safely used. In this context, a seismic event is defined by :

- Its occurrence time
- Its location in space, which is in natural context usually along faults
- The moment tensor of forces exerted during the event, which gives both an estimate of the strength of the seismic event (the moment magnitude) and in which directions these moments were applied (focal mechanism). Focal mechanism can be separated into double-couple moments where the volume does not change, ie moments parallel to a fault surface, and non double-couple moments for which the volume can change ; for natural events, the source is overwhelmingly double-couple.
- The moment magnitude for small events can be linked with the peak frequency of their spectral content, and with the typical size of the rupture

Once a seismic event is occurring, compression and shearing mechanical waves (dubbed P and S waves) propagate from the source with an initial radiation pattern directly linked to the moment tensor. Like other types of waves, this propagation is affected by the local speed encountered ; this speed is linked to bulk and shear modulus of the rock that describe how mechanically “strong” the rock is depending on the sollicitation

Seismic events are detected with seismometers. These instruments are recording ground movements resulting from various sources, natural or anthropic. Seismometers have various characteristics making each instrument brand unique, but can roughly be classified using the following categories :

- Long period (> 60 s) displacement measuring instruments and velocimeters are used for global seismology and are unsuitable for microseismicity monitoring
- Broadband velocimeters have a typical frequency range between 60 s and 100 Hz, and are frequently used as surface sensors for regional events and networks (although some models can be deployed in observation wells)
- Geophones cover the high end of the seismic spectrum (from 1 Hz-10 Hz depending on the model to several hundred of Hz) and are deployed either on the surface or in observation wells either definitively cemented or simply clamped ; because of their compacity, their lower price and their frequency range suited for microseismic events, they are the most commonly used seismometers for microseismicity monitoring for geothermal exploitations.

- Strong motion accelerometers are used where strong events are expected, as they can sustain bigger ground movements while velocimeters can be saturated ; they are able to measure high accelerations (up to several G) at the expense of amplitude precision and lessened sensitivity. These seismometers are therefore used for seismic risk purposes and are not suited to geothermal exploration.

Seismometers can be locally regrouped into arrays that
Seismometers are regrouped into a network. The size of a network may vary with the area to be explored (from regional networks to local ones), and may include with current tools several types of instruments deployed either in individual stations or in local arrays that allow a better sensitivity and a better azimuthal precision.

4.2.1.2 Benefits

By definition, the location of microseismic events shows where the active faults are, and with enough events what approximate direction the fault plane is ; their radiation pattern is directly linked with the fault plane orientation, and their amplitude can lead to estimates of stress drops and therefore hint at the regional and local stress state. Observing local microseismicity is therefore one of the main tools to understand the stress state and the faults orientation that will greatly influence the choices for the exploitation.
Microseismic monitoring and regional/global events recordings, given enough events and stations, can also be used to constrain the 3D velocity model with joint inversions and P/S tomographies. This 3D model can then be used to complement/replace 3D seismics and get an image of the target site, better constrain the position of events in the exploitation phase, and monitor velocity changes occurring during the exploitation phase because of fault openings and new fluid circulations.
Contrary to 3D active seismic acquisitions, passive seismic networks do not require a heavy deployment campaign with the associated permitting problems. A surface station occupies less than one square meter of land, making the negotiations with the land owners far easier ; observation wells, while taking some place in the drilling phase, are not actively used thereafter and thus have a less visible footprint.
Finally, seismic networks for microseismic monitoring can be reused as such for the exploitation phase, and the initial investment is therefore to be considered for the entire duration of the project and not only the exploration phase.

4.2.1.3 Resolution

The resolution of the network depends on the station layout and density, the nature of the sensors and their position, as well as the nature of the surroundings. As such, no precise answer can be given unless a case study is properly carried out. However, the long seismological experience shows that some a-priori estimates can be done for different types of networks.

4.2.1.3.1 Temporal and spatial resolution

For epicentre (the point at the surface above the seismic event) and occurrence time, two basic cases can be distinguished :

- the considered event takes place inside the network : for regional networks, the epicentre position is defined within a few hundred meters, and below one hundred meters for local networks. The occurrence time can be defined within 10 ms.
- the considered event takes place outside the network : the position and time error rapidly increases as the event is further away from the network, to the point that no useful information can be extracted from the best estimate position.

It is therefore of utmost importance to correctly design the network in order to encircle the zone of interest
Depth resolutions are as follows :

- with surface only networks, depth estimates are usually poorly constrained (at least 3 or 4 times the horizontal error) even with azimuth measurements that can be obtained with 3-component sensors or arrays

- networks with stations deployed deep enough in observation wells (ideally at the depth of the target zone) have a much better resolution in depth, usually below 100 meters. This gain is only possible with local networks surrounding a limited area of interest and not for regional networks

It is possible to improve the spatial resolution of events relative to each other with relocalisation methods (see Waldhauser 2000) : by selecting a "master event" and relocating other events relative to the first one, one can this way better map the active faults. This is therefore a powerful and useful method when enough events (more than one hundred) are recorded in the area.

4.2.1.3.2 sensitivity to event magnitude

Passive seismic networks can only record events strong enough so that seismic waves arriving at the station have enough energy to overcome the background noise. This capacity varies for each network depending on the surrounding area (peri-urban conditions, presence of trees, etc.) and should be studied specifically for each network ; however, some rules of thumb can be defined :

- for regional networks, the minimum magnitude recorded is usually around 2
- for local surface networks, this magnitude is around 0
- for networks with subsurface stations (ie stations in observation wells at a depth of 100 m or below), the minimum magnitude can go below -1 or even -2 ; this is due to the fact that the weathered zone (the deeply altered zone at the surface) dampens seismic waves and that background noise is mainly generated at the surface, making the surface stations inherently less sensitive
- networks with stations directly in the target area have a magnitude sensitivity going down to -4 ; however, deploying stations at depth can be costly for usual EGS targets (several kms)

4.2.1.3.3 tomography resolution

The spatial resolution of tomographic inversions from wave arrivals is overwhelmingly dependant on the station density ; as such, one can estimate that the typical resolution is approximatively equal to the average interstation distance. Seismic events have however to be correctly distributed, otherwise the resolution can be greatly reduced.

4.2.1.4 Limitations

Obviously, this method is limited to the observation of *active* faults ; faults without any seismic activity are invisible to microseismicity monitoring. This method also requires that enough events are recorded ; given that the operators have no control over natural seismicity, seismic networks must be deployed a time long enough. Usual deployments can span months, or even years.
As passive seismic networks have usually far less stations than active seismic lines, the resolution obtained is lower than usual 3D active seismics and cannot map precisely faults through velocity tomography. Finally, background noise conditions greatly influence the network sensitivity, making this method less effective in urban conditions to the point that sometimes only night data can be exploited.

4.2.2 Ambient Noise Tomography

4.2.2.1 Principle

Seismometers record ground movements generated not only by earthquakes but also by a vast variety of sources (ocean waves, trees, anthropic activity, tremors, etc.) historically categorized as "noise". These sources generate mainly surface waves ; the speed of these waves changes with frequency and are linked with the velocity profiles encountered, allowing for inversions of velocity profiles.

Several methods have emerged over time to exploit the datas generated by seismic noise :

- local arrays can be deployed to measure 1D velocity profiles from phase speed of surface waves crossing the array (Aki 1957) through several methods : (modified) spatial autocorrelation, (high resolution) frequency-wavenumber analysis. This method is often used in volcanology and in the Comprehensive nuclear Test Ban Treaty Organisation framework to assess the local velocity profile under the seismic array deployed to measure events
- Single stations can be used to measure horizontal to vertical energy spectrum ratio extracted from surface waves passing by ; this ratio is linked to the velocity profile, especially the interfaces with an important velocity contrast. H/V measurements are mainly used in seismic risk to assess peak frequencies and therefore frequencies for which buildings are at risk, but are of little use to velocity profile estimations as the associated inversion process is severely underdetermined.
- Finally, seismic noise recorded by stations in a network can be used to retrieve surface waves crossing the network (Shapiro and Campillo 2004) as well as body P and S waves (Roux et al 2005) : one station acts as the virtual source, while the others act as receiver. It is possible this way to retrieve from a N stations network up to N(N-1)/2 surface wave raypaths, thus allowing a 3D tomography with enough stations. This method was used to map for example the San Andreas basin, the European Moho or the Piton de la Fournaise volcano, showing its capacity to map great depths with a correctly designed network. While networks for these cases lasted for several years, recent studies suggest that the amount of time needed is not so important (at most some months)

4.2.2.2 Benefits

Local array networks using MSPAC and F-K methods give good estimates of 1D S speed profiles with a light deployment for a short amount of time (one or two days). This profile can complement P speed profiles obtained from active seismic and therefore give a full mechanical picture of the target area.

Long range tomography with passive seismic networks is able to cover vast areas spanning several kilometers or even several dozen of kilometers (see above) with a very reasonable cost compared to active seismic lines. Most broadband stations are currently able to function autonomously with a small power consumption and can (with the correct equipment) broadcast easily their data either through local Internet lines or 3G/satellite connexion, thus needing a smaller technical overview during the deployment.

Surface stations used for ambient noise tomography occupy far less space than active seismic lines and therefore are less visible and better accepted, even for long durations – these methods can therefore be deployed where active seismic methods are forbidden, and can begin a positive discursive loop with local population and authorities.

Finally, networks used for ambient noise tomography can also be used during the same time for microseismic monitoring, thus allowing the use of several methods with one network.

4.2.2.3 Resolution

4.2.2.3.1 Horizontal resolution

MSPAC/FK measurements are point measurements, ie one array is able to retrieve the vertical speed profile below. Horizontal resolution is therefore entirely dependent on the number of arrays measurements done, and can be scalable ; however, since the penetration depth is linked to the array extension (approximatively diameter = 2 times the depth), one cannot expect an better precision than a few hundred meters.

Ambient noise tomography resolution, like arrival time tomography resolution, is highly dependant on the station disposition and density. The maximum theoretical resolution (with an infinite number of stations) is equal to the Fresnel volume occupied by the surface wave, which depends on the

frequency considered. For practical reasons, horizontal resolution for this method can not go below several hundred of meters.

4.2.2.3.2 Maximum possible depth

For all methods relying on surface waves, penetration depth is directly linked to the lowest frequency measurable, which in turn depends on the distance between stations. One can approximate that the maximum depth possible is half the distance between stations.

4.2.2.4 Limitations

The main limitation of the ambient noise tomography method is its limited spatial resolution, making it suitable only for regional explorations ; on local sites, the precision is far below what is needed to correctly characterise the area.
MSPAC/FK methods require increasing diameters to go deeper ; for most applications, the diameter is not greater than 1 km, although it is not clear whether the method is limited or the previous uses did not need a greater depth range.
Ambient noise tomography, because it relies on measurements between station pairs, needs a minimal amount of station deployed simultaneously to work properly ; in order to get the frequency range needed to retrieve velocity for the deep targets envisioned by EGS (several kms), broadband stations are mandatory. Since the cost of a broadband station is far higher than the cost of a simple geophone, the initial investment is more important, but can be compensated by the cost savings later.
Finally, these methods are not commonly met outside academic researches, and are therefore not mastered by everyone.

4.3 Electro-Magnetic

4.3.1 Electric Resistivity Tomography (ERT)

4.3.1.1 Principle

The electrical resistivity tomography is an active geophysical technique (DC artificial source,) which uses the capability of a terrain to conduct an electrical current, in order to probe subsurface electrical resistivity variations. This physical property is directly related and sensitive to the type of rock investigated, the clay content, the fluid and its ions content, and therefore, other physical properties such as porosity and permeability can be inferred (for example with Archie's and some limitations) from these measurements.

The electrical resistivity method involves the measurement of the apparent resistivity of soils and rocks as a function the geometrical configuration of two pairs of electrodes. Current is injected into the earth through a pair a current electrodes (generally called "A" and "B"), and a potential difference is measured between a pair of potential electrodes (generally called "M" and "N").

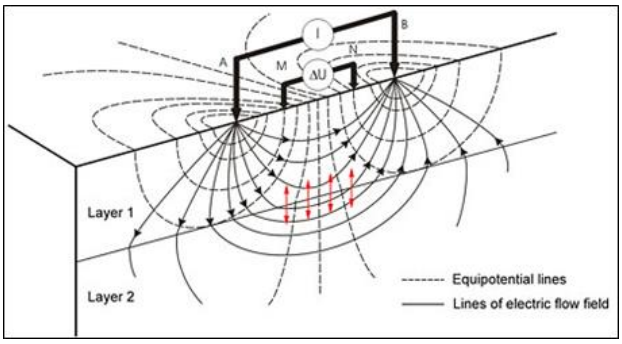

Figure 30 : Principle of an electrical sounding, with current distribution

The current and potential electrodes are generally arranged in a liner array providing a 2-D tomography of the ground. Common arrays include Dipole-Dipole array, Wenner-Schlumberger array, Pole-Dipole any many other 2-D or 3-D configurations do exist. The apparent resistivity is the bulk average resistivity for a single quadripole ABMN. Merging the apparent resistivity of several quadripoles provides a pseudo-section of measured apparent resistivity. Through the process of inversion (1-D, 2-D or 3-D), it is possible to recover a (1-D, 2-D or 3-D) a subsurface electrical resistivity distribution whose calculated apparent resistivity matches as much as possible (misfit) the measured apparent resistivity.

4.3.1.2 Benefits

Due to technical development in the last decades, the old standard Schlumberger sounding that required four independent electrodes has moved to useful multi-electrodes systems providing up to 96 electrodes (or more), allowing a quick acquisition procedure of any programmable configuration. This flexible technique has become an unavoidable geophysical tool and has been successfully used for many environmental problematics. Particularly, ERT technique has been implemented for hydrogeological applications (delimitation of aquifers, aquitards, contamination of groundwater, salt water intrusions), geological applications (lithological contrasts, structural objects), soil properties, mining exploration, archeological applications, landfill application, detection of underground structures such as cavities, superficial geothermal applications, and many others. In most cases, common acquisitions range from metric scale up to kilometric scale with depth penetration ranging from tens of centimetres up to few hundred of meters but can be much more according to the configuration.

The equipment is relatively light, portable and not so expensive. A qualitative interpretation of the data is rapid and straightforward. Final expenses are minimal with respect to the cost of drilling or remediation procedures, for example. The technique is commonly used in 1D, 2D or 3D survey with standard procedures for both acquisition and inversion.

4.3.1.3 Resolution

As for electromagnetics, resolution of ERT decreases with depth and must be studied in details before planning a survey. It is crucial to understand how much the resistivity image will resemble the object, what artefacts can be expected to arise from propagation of data error on image noise and how can the design of measurement and inversion be optimized to achieve maximum information. In particular, the resolution is strongly dependent on the depth of the target, its size and geometry, on the resistivity contrast with surrounding rocks and the adopted acquisition configuration. Prior forward modelling can be done “easily” with standard free software such as Res2Dmod.

It is not possible to explore all possible cases study with different acquisition configuration. Below is shown a typical example (of a shallow geothermal application) where the target is a 1 Ωm fault (supposed to be conductive), 20 m width, embedded in a host rock of 20 and 1000 Ωm. The overburden is composed of two layers : 2.4 m of soil (10 Ωm) overlying 27 m of terrain at 100 Ωm. A dispositive of 96 electrodes with 20 m spacing has been selected to cover a profile of 1900m and reach a depth penetration of about 400 m. Forward model is computed for the Wenner-Schlumber and Dipole-Dipole arrays and 5.00% of noise in added to the synthetic data before inversion.

Inversion is performed using Res2Dinv (Loke and Barker, 1996). These results show that the Wenner-Schlumberger configuration recover pretty well the tabular structure of the medium, however it is difficult (without external constrains) to precisely locate the top of the deep resistor (top of the yellow at ~100 Ωm), because of the smooth resistivity gradient. The soil layer is not present because of the large electrode spacing (20m). Finally, the target is well resolved in the first 120 m but is not visible anymore below. After enlarging the fault zone to 100 m width, or merging the 20 Ωm and 1000 Ωm zones in a single one at 1000 Ωm, the fault at depth remains not visible.

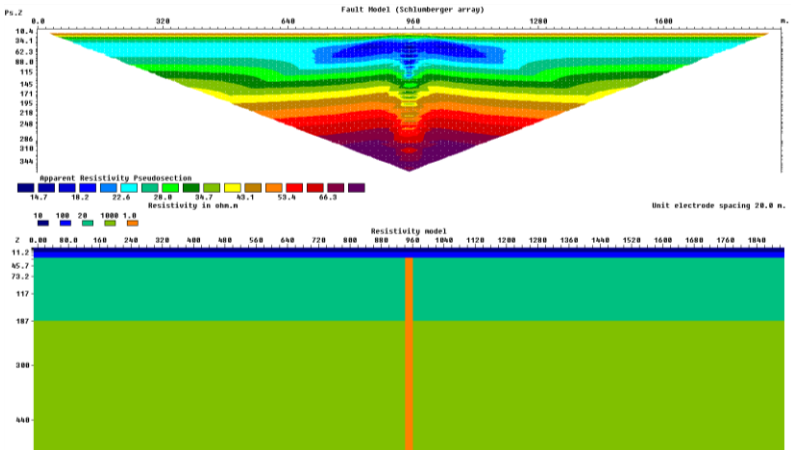

Figure 31 : Resistivity model (bottom) and forward modelling response (top) for the Wenne-Schlumberger configuration

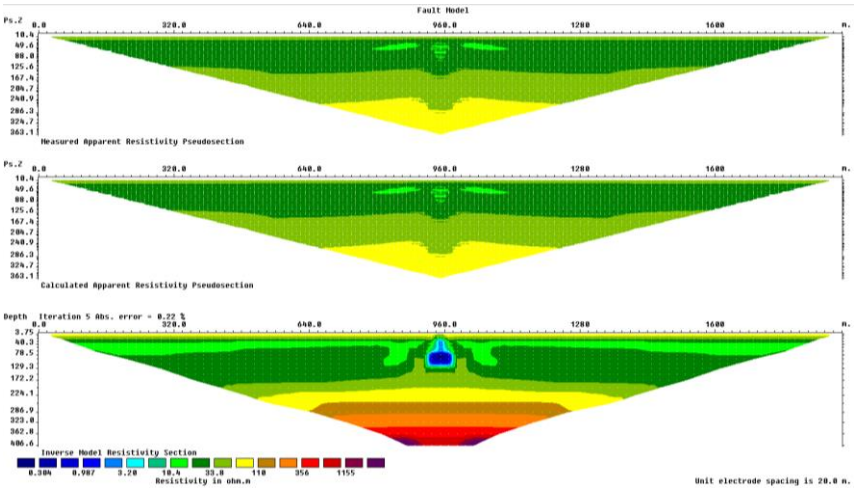

Figure 32 : 2-D inversion of the pseudo-section of apparent resistivity (previous figure). Bottom: resistivity model.

Moving to the dipole-dipole configuration, we can observe that the vertical conductive structure is well recovered all over the section and top of the resistor is much more defined than in the previous WS configuration.

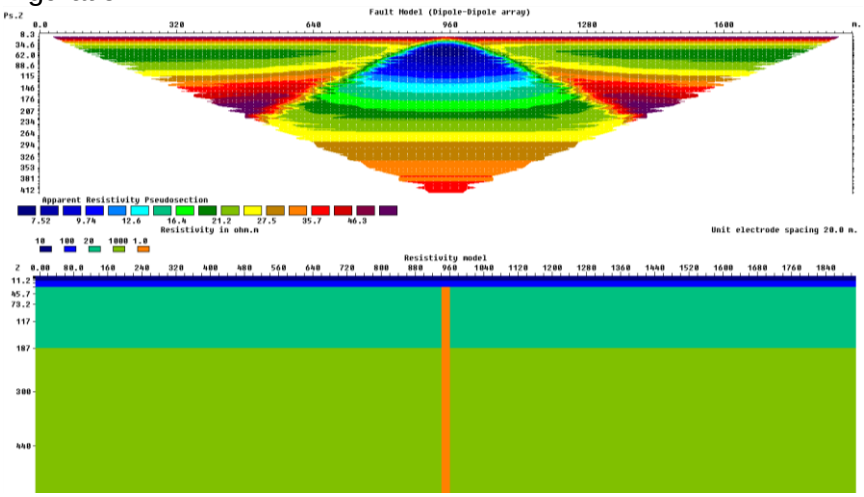

Figure 33 : Resistivity model (bottom) and forward modelling response (top) for the Dipole-Dipole configuration

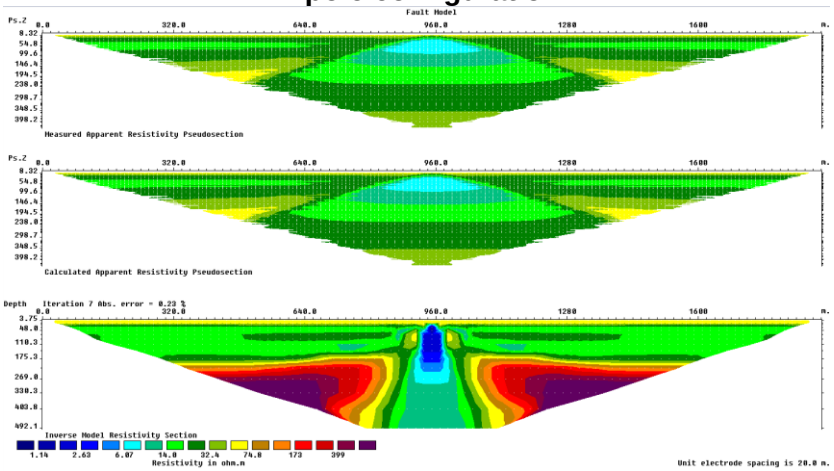

Figure 34 : 2-D inversion of the pseudo-section of apparent resistivity (previous figure). Bottom: resistivity model.

In practice, this is explained by the difference of sensitivity of these two configurations when probing the earth. Assuming that the measured signal is sufficient to be measured on all selected levels for the Dipole-Dipole configuration, we can observe that the Dipole-Dipole is much more sensitive to vertical resistivity contrasts while Wenner-Schlumberger is a more integrative configuration, resulting in smoother resistivity model.

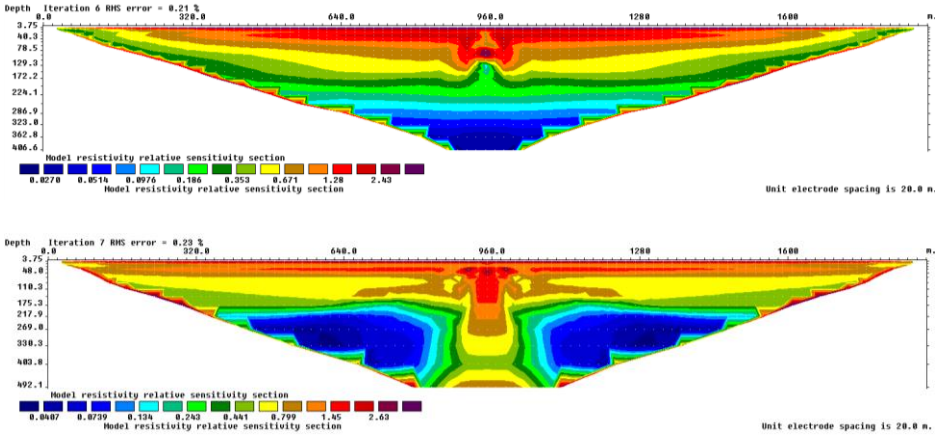

Figure 35 : Representation of sensitivity matrix for both Wenner-Schlumber (top) and Dipole-Dipole (bottom) arrays.

4.3.1.4 Limitations

As stated above, the resolution decreases with depth. Therefore, target size (and resistivity contrasts) must be carefully studied before designing an ERT survey. Deeper the target, bigger it should be and/or higher the contrast with surroundings rocks must be. Accuracy of depth determination is lower than with seismic techniques for example.

When greater depth of investigation is required (below 200 m deep, which is the approximate depth of investigation of a standard 1 km long profile), implementation of such technique requires space (and therefore more authorizations, security, equipment and time).

Finally, as for many geophysical techniques, the principle of non-uniqueness of resistivity models applies. This means that many resistivity models can fit the same dataset. Therefore, the more external constrains (boreholes, geophysical logs, and so on…) that can be integrated into the inversion (and interpretation), the more accurate will be the model and the understanding of the medium. Without a priori knowledge, interpretation of complex geologic structures can be difficult and ambiguous, especially in 3-D context. Also, presence of metal pipes, cables, fences and electrical grounds can complicate interpretation.

4.3.2 Magneto-Tellurics (MT)

4.3.2.1 Principle

In the magnetotelluric (MT) method), natural electromagnetic fields variations are used to investigate the electrical conductivity structure of the earth. Natural sources of MT fields above 1 Hz are thunderstorms worldwide, from which lightning radiates fields which propagate to great distance. At frequencies below 1 Hz, the bulk of the signal is due to current systems in the magnetosphere set up by solar activity.

In both cases, the electromagnetic (EM) fields at the surface of the earth behave almost like plane waves, with most of their energy reflected but with a small amount propagating vertically downward into the earth. The amplitude, phase, and directional relationships between electric and magnetic fields on the surface depend on the distribution of electrical conductivity in the subsurface. By use of computed models, field measurement programs can be designed to study regions of interest within the earth from depth of few tens of meters to the upper mantle.

On the field, MT measurements consist in installing two orthogonal electric dipoles with non-polarisable electrodes to measure the horizontal components of the electric field, and three magnetic sensors to measure horizontal and vertical components of the magnetic field. Due to the technical improvements the last decades, these five components are now recorded simultaneously during periods of minutes to days, according the highest and lowest frequencies requested to probe correctly the target and the medium.

In a common use, a MT station (remote reference) is installed far away (in a quiet area with expected local noise different from those of the study area) from the study area during the survey with the aim to correct and improve data quality during processing using magnetic components. In addition, Time-Domain ElectroMagnetic (TDEM) measurements are performed at each MT station to correct for static shift effect and therefore adjust MT resistivity at high frequencies to the resistivity model obtained by TEM. Many techniques have been proposed to solve this problem.

4.3.2.2 Benefits

Using natural electromagnetic sources, the magnetotelluric method can be considered as the “green” geophysical technique. Moreover, and because strong enough transmitter are not commercially available, it is actually the sole technique able to probe electrical resistivity at depth of several kilometres.

4.3.2.3 Resolution

To illustrate the resolution that can be expected from MT measurement we simulate a massive conductive body (3 km x 3 km, 500 m thick) embedded in a homogeneous 100 Ωm medium using WinGlink software (Geosystem). The response of the homogeneous model is first computed. Then, MT responses including the conductive body from 1000 m down to 5000 m depth are computed (nine models) (Figure 36). Results of three MT sites (S61, S63 and S66) are presented.

Figure 37 shows apparent resistivity and phase curves for both Zxy and Zyx polarisations. The following main elements that can be appreciated on this figure are :

- Deeper the anomaly, lower are the frequencies which do reflect it and smaller its amplitude.
- The superposition of both polarisations on site S61, due to its central position with respect to the conductive body. All 3-D effects are compensated and sounding is 1-D (particular case).
- The clear 3-D effect, induced by the conductive anomaly, on site S63. Curves blue and red (1000m) are the results of the same model but probing electromagnetic field in perpendicular directions. This case illustrates the complexity of reconstructing a reliable resistivity model if one polarisation is of bad quality (for example) or if the density of MT soundings is not sufficient.
- 5 km away from the centre of the conductive body (S66), the amplitude of the anomaly has strongly decreased and is now very tenuous for periods longer that 1s. It can therefore be very tricky and speculative to highlight it in noisy data.

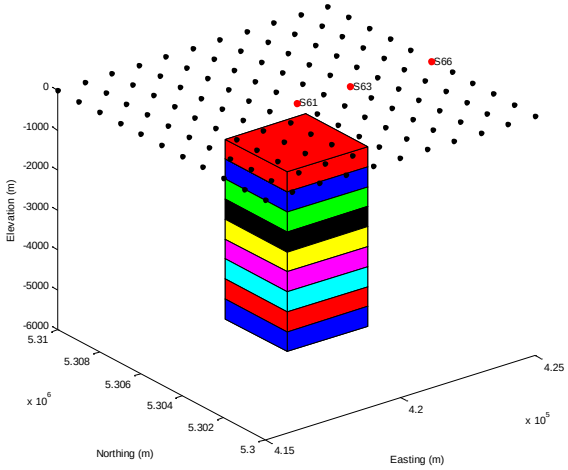

Figure 36 : Resistivity model. A conductive body (1 Ωm), 3 km width, 500 m thick embedded in a homogeneous medium of 100 Ωm is moved from 1000 m depth (top of the body) down to 5000 m depth by step of 500m.

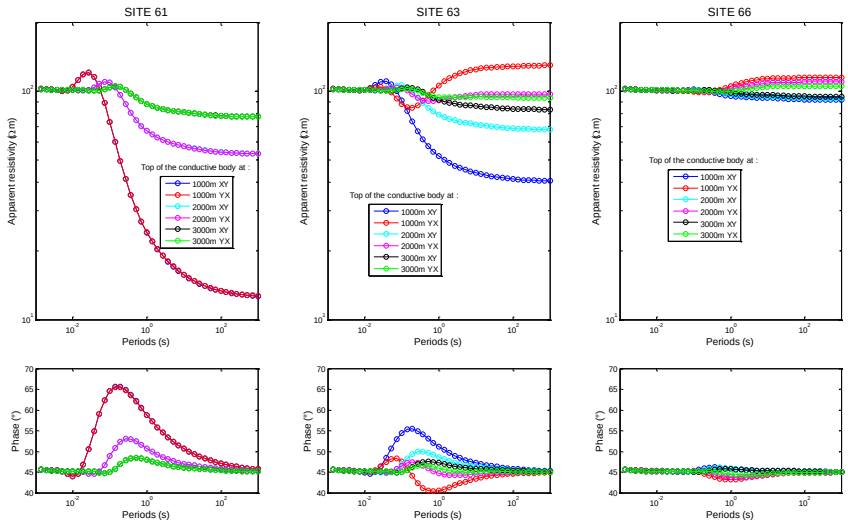

Figure 37 : Off-diagonal components (Zxy and Zyx) of the MT impedance tensors MT of soundings S61, S63 and S66 for 3 model configurations (top of the conductive body located at 1000, 2000 and 3000 m depth).

Then, apparent resistivity variations and phase differences with respect to the homogeneous model are calculated and presented for 3 sites located at the centre of the anomaly (S61), and at 2 km (S63) and 5 km (S66) from S61. Here is only presented and discussed the polarisation XY constructed with electric field Ex and magnetic field Hy. Colors of the conductive block (Figure 36) do correspond to colors of curves responses (Figure 38, Figure 39 and Figure 40).

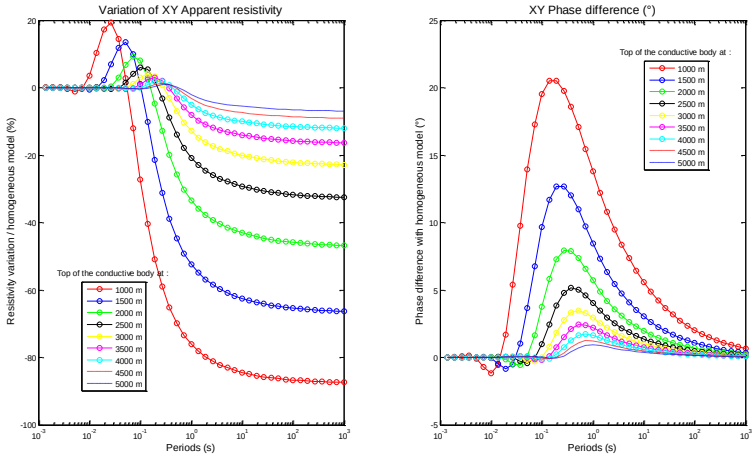

Figure 38 : Site S61. Apparent resistivity variations and phase differences for 9 models resistivity models (XY polarisation).

The resistivity variation is computed as $(\rho_1 - \rho_0)/\rho_0$ and the phase difference as $\varphi_1 - \varphi_0$. As expected resistivity variation and phase difference strongly decrease as the conductive body deepens. Also, maximum amplitude of the resistivity variations and phase difference moves towards longer periods.

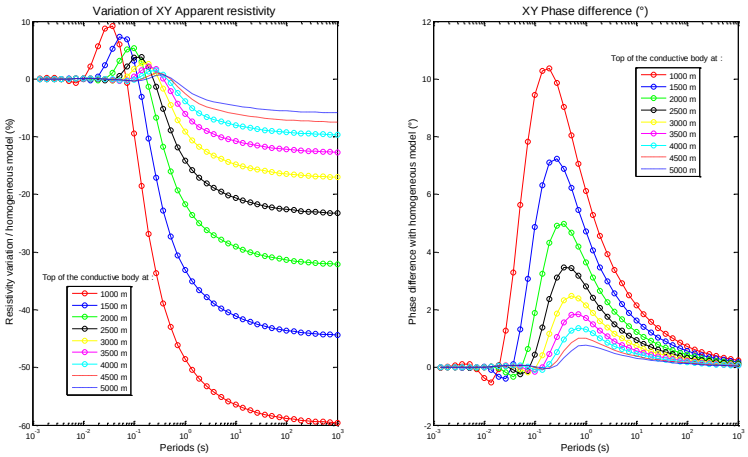

Figure 39 : Site S63. Apparent resistivity variations and phase differences for 9 models resistivity models (XY polarisation).

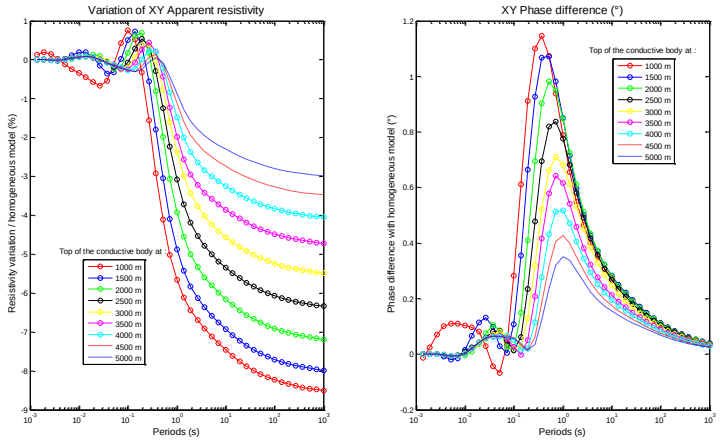

Figure 40 : Site S66. Apparent resistivity variations and phase differences for 9 models resistivity models (XY polarisation).

When comparing to the CSEM model used for resolution example (with a conductive body of 1 km, 100 m thick), the phase difference between the homogeneous model and a conductive body located at 1500 m depth is maximum for site 61 at about 10 Hz and is equal to 1%. The apparent resistivity variation reaches 6 to 7% between 1s and 1000s. All other data are below.

What resistivity information can be retrieved from these different datasets? To simplify, only two 2-D standard smooth inversions (WingLink, Geosystem) were carried out taking into account 11 stations (S56 to S66) along a O-E profile, passing by the centre (site S61) of the area. The data from conductive anomaly located at 2500m and 5000m were selected. Figure 41 shows the resistivity model obtained after inversion of synthetic data computed with the 1 Ωm conductive body located at 2500 m depth. Due to the fact that we used synthetic data, final RMS and data misfit are very good. Note the final resistivity range (24-130 Ωm) which is quite different from the original (1 and 100 Ωm for the background) and especially the resistivity of the conductive body which has strongly increased. In terms of interpretations for example, this might be very critical without any other data constrains (resistivity log, geological model, seismic data,…). This also indicates that in case no strong external constrains can help to understand the results, additional forward modelling will be necessary to better understand the data and mature the interpretation.

Also, the size of the conductive anomaly (especially its thickness, vertical resolution) has significantly increased (depending where interpreter would position its vertical boundaries).

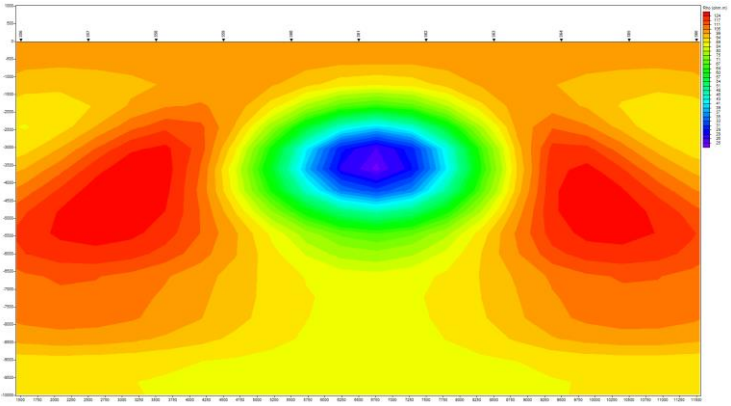

Figure 41 : 2-D resistivity inversion of synthetic data (model with conductive body at 2500m depth). TE and TM mode inverted over 6 decades (0.001 Hz to 1000 Hz). Black box is the conductive anomaly of the original model.

The second resistivity model (Figure 42) is presented to illustrate the general trend of what can be expected when target deepens. There, the centre of the anomaly is pretty well located but locating its lateral and vertical boundaries would be very difficult since gradient is rather continuous. The resistivity contrast between the target and the background is reduced to 20 Ωm. Looking at the synthetic data, the maximum resistivity variations (on site S61) is of few % only (Figure 38), which is quite small and probably visible only in very high quality field data. Synthetic noise could also be added to test the inversion limits of such synthetic data.

Globally, deeper the target, lower will be the resistivity contrast, larger will also be the returned anomaly. In these models, a contrast of 100 has been chosen, but it can be much lower in many applications, with consequences on resolution. Due to the diffusive behaviour of electromagnetic waves and as a rule of thumb it is difficult with real data to find objects which are 10 times smaller than the depth at which they are embedded (here the case with the deeper conductive body).

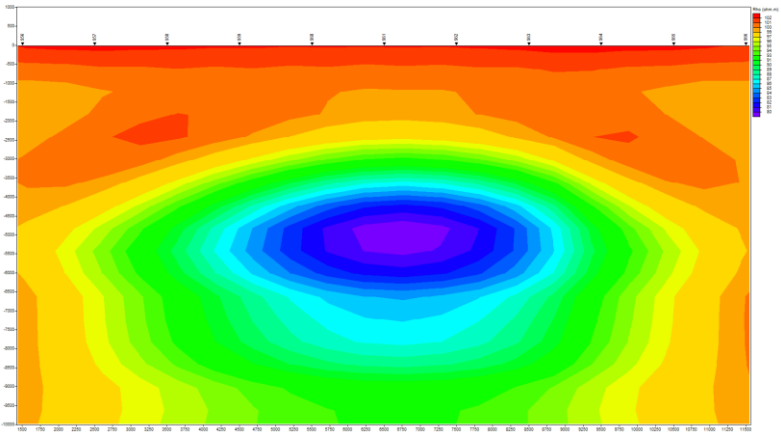

Figure 42 : 2-D resistivity inversion of synthetic data (model with conductive body at 5000m depth). TE and TM mode inverted over 6 decades (0.001 Hz to 1000 Hz). Black box is the conductive anomaly of the original model.

4.3.2.4 Limitations

One of the main limitations of the MT technique is related to the diffusive nature of the EM waves. Indeed, as shown in the previous section, it struggles to detect small bodies at great depth due to the strong attenuation of the EM waves but also to differentiate between a heterogeneous medium and its up-scaled equivalent (e.g. objects of similar transverse resistance). Resolution is also dependent on the spatial coverage of the survey (number of MT stations).

As stated above, the magnetotelluric method also strongly suffers from anthropic noise which may irrevocably degrade data quality even when one (or more) remote reference is used. Therefore, noise conditions should be investigated prior any MT survey. Such noise are caused by power lines (50 or 60 Hz), train, DC train, antennas, buried metallic structures, metallic pipes, any anthropic activity susceptible to generate disturbances in the frequency band 1000 s to 10 kHz. Therefore, in the vicinity of main cities, where expected geothermal resources need to be investigated, general experience suggests that MT should be discarded.

Moreover, since solar activity is only predictable for short term (few days) and periodic 11 years cycles affect the MT signal, it can be difficult at a given period, and in noisy environment to collect good data quality. In some countries or places, collecting authorizations to access all measurement sites can be time consuming. Many mathematical techniques allow to improve more or less artificially the data quality, there a great attention must be paid to the original data quality to assess the reliability of the proposed resistivity models.

Whether if 3-D MT inversion is now commercially available, blind-test carried out using different software show that recovering complex resistivity distribution can be a tricky task. Finally, as for many geophysical techniques, the principle of non-uniqueness of resistivity models applies. This means that many resistivity models can fit the same dataset without external constrains (boreholes, geophysical logs, and so on…).

4.3.3 Controlled-Source Electro-Magnetics (CSEM)

4.3.3.1 Principle

The CSEM survey or method uses electromagnetic field generated in the subsurface using a controlled source (usually a highly powered electric dipole) and measured at different offset locations using EM receivers (usually MT receivers) to infer the subsurface resistivity variations (Figure 43).

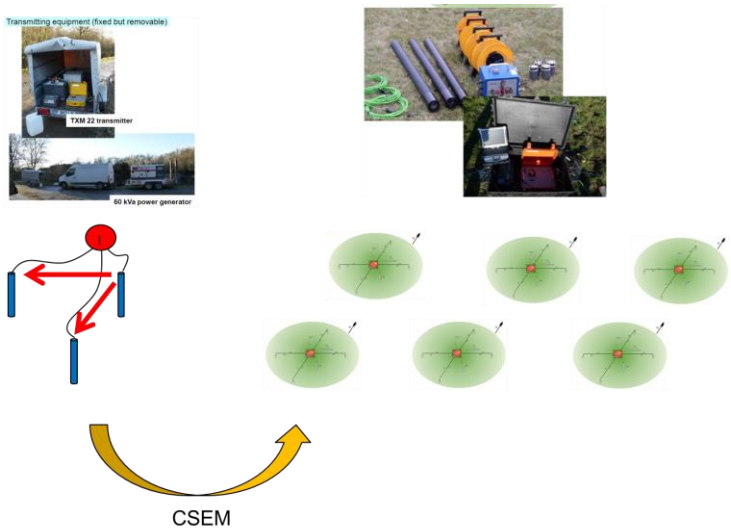

Figure 43: Controlled Source Electro-Magnetic (CSEM) principle

4.3.3.2 Benefits

The benefits of using CSEM methods are similar to the MT method; expect that this technique is much less sensitive to external sources of EM noise (e.g. industrialized areas) and to the variability of the EM source (solar wind/lightning of the MT method). It is therefore well-suited for geothermal exploration in industrialized areas in order to map subsurface resistivity variations at target level. An example in Belgium is shown on where the target was to map the depth and resistivity of deep carboniferous limestones.

4.3.3.3 Sensitivity and Resolution

Due to the relatively low conductivity of sediments (<10000 Ω.m) and the depth of geothermal targets (>2km), low frequencies EM have to be used in the CSEM method (<1000Hz). At these frequencies, the EM fields are strongly attenuated in the Earth and diffuse. To characterize this diffusion/attenuation, it is classical to use the concept of skin depth, defined as the distance over which the EM wave has lost 1/e (~63%) of its energy. The skin depth has the following expression:

$$\delta = 503\sqrt{\rho/f}$$

where ρ is the resistivity of the medium (Ω.m) and f is the frequency (Hz). The lower the frequency, the longer the skin depth and hence deeper the EM wave penetrates the earth (Figure 44). However, the lower the resistivity, the smaller the skin depth and hence the shallower penetrates the earth the EM. It demonstrates why the resistivity of the sediments is the key parameter governing how deep the CSEM sounding can sense. The resistivity of sediments overlying deep geothermal reservoirs can be very variable: either very conductive (<10 Ω.m) like marls, brine-filled

sandstone or very resistive (>100 Ω.m) like limestones, salt. The frequencies to be used and hence the spatial resolution of the technique is therefore very dependent on the geology of the sedimentary cover. This must be assessed with a forward modelling study on a case-by-case basis. It is also important to realize that the lower the frequency, the higher the MT signal (or noise here) and hence the longer the EM recording times need to be to stack out EM noise (and hence the more expensive the survey is).

Since EM waves do not propagate at the CSEM frequencies, we cannot use the concept vertical/horizontal resolutions based on wavelength as used in the seismic section. Instead, we introduce the concepts of sensitivity and resolution based on forward modelling (as it is going to be case-by-case specific). The sensitivity is defined as the ability of a CSEM measurement to detect a certain change of resistivity of certain size and at depth given a certain measurement error and noise level. On the other hand, the resolution is defined as the ability of a CSEM measurement to distinguish between two objects of a certain resistivity, size and depth given a certain measurement error and noise level.

An extra degree of complexity of the CSEM method is related to the fact that the CSEM technique does not illuminate the subsurface homogeneously and therefore the CSEM sensitivity varies in 3D. Figure 45 illustrates this aspect in a homogenous medium where a conductive anomaly is moved around a certain source and receiver position. The shallow section underneath the source and receiver is where the sensitivity is highest while at depth and in between the source and receiver, the sensitivity decreases. The shape of the sensitivity pattern is however very complex and cannot be predicted easily as it depends on many parameters (source/receiver offset, frequency, background/anomaly resistivity and size of the anomaly).

To simplify the problem and look into the sensitivity/resolution of the CSEM technique, we assume that the conductive anomaly is located underneath the receiver (or source as reciprocity principle holds). Figure 46 shows the variation of the CSEM anomaly as function of the depth and size of a 1 Ω.m 100m thick conductive anomaly embedded in a homogeneous 100 Ω.m half-space, simulating a conductive fault zone in rather resistive sequence of sediments. The smaller and deeper the anomaly, the smaller the CSEM anomaly is. The relative and absolute anomalies were intentionally cut-off at 0.1% and 10^{-14}V/A.m^2, respectively as we consider that such anomalies are beyond today's CSEM capabilities. For such a resistivity contrast, 100m thick objects smaller than 500m width at 3km depth cannot be detected, while 100m thick objects smaller than 1km at 5km depth cannot be sensed.

Figure 47 shows the relative and absolute CSEM anomaly for a 100m x 100m wide box of variable resistivity and height embedded in a 100 Ω.m medium. The thicker and the less resistive the object, the higher the CSEM anomaly is. It is however interesting to observe that models with similar transverse conductance (conductivity times thickness or 1/resistivity times thickness) give rise to equivalent CSEM anomalies (e.g. 1 Ω.m 50m thick ~ 3.1 Ω.m 200m thick ~ 10 Ω.m 500m thick). Such objects can therefore not be differentiated with CSEM data.

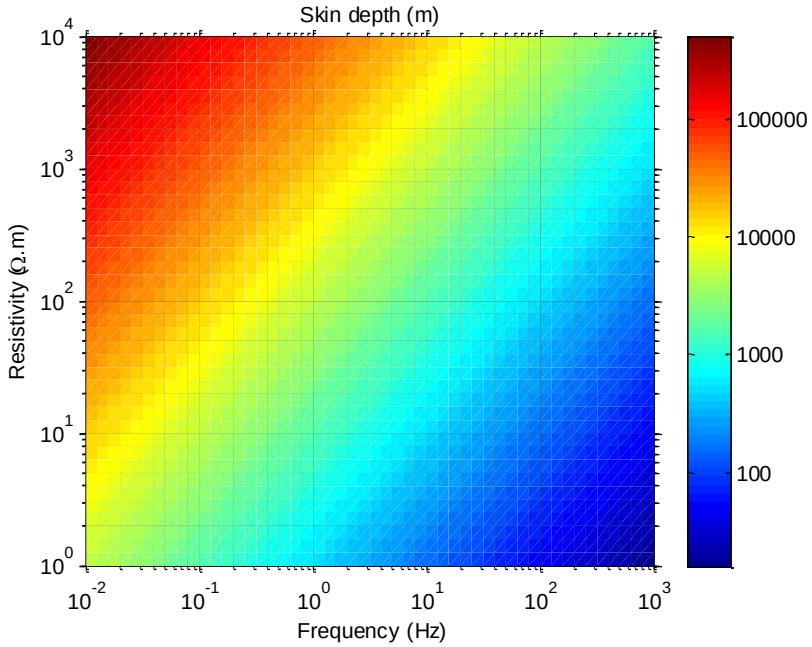

Figure 44: Skin depth as a function of the EM wave frequency and resistivity of the medium.

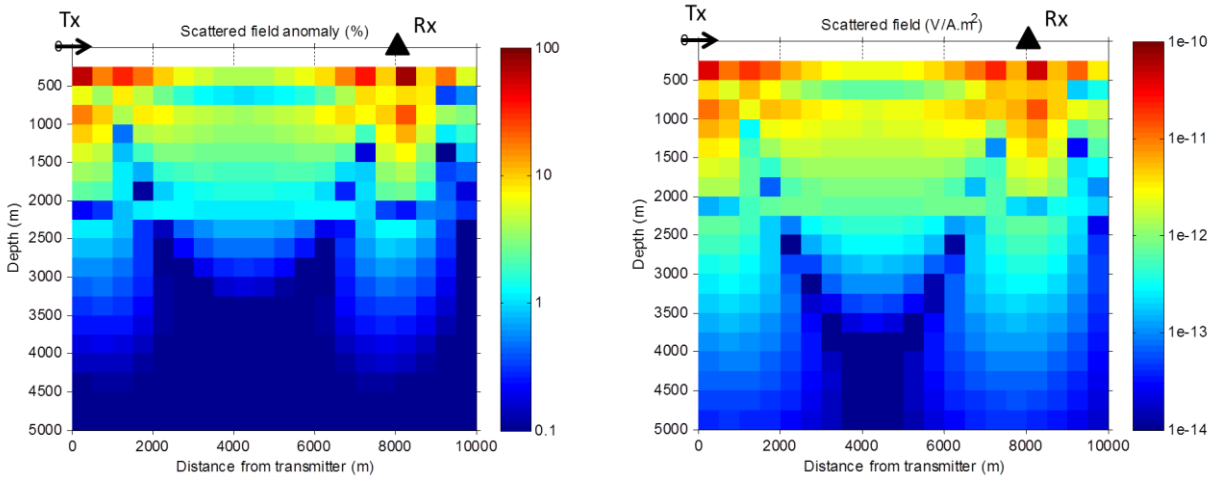

Figure 45: Relative (left) and absolute (right) CSEM anomaly for 1 Ω.m box of 1km width x 100m height of variable distance and depth from the transmitter, embedded in a 100 Ω.m medium for a CSEM receiver located 8km from the CSEM source at 16s (0.0625Hz).

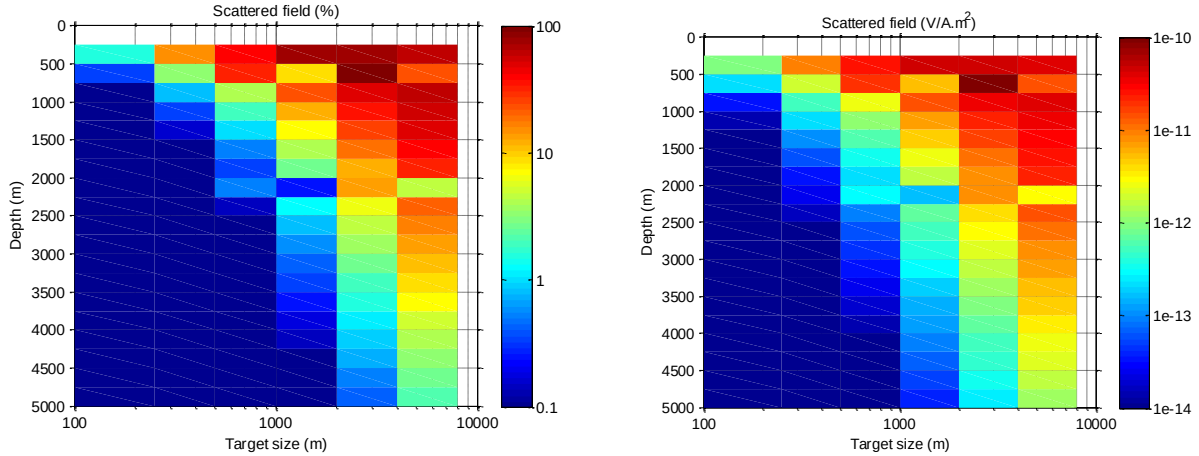

Figure 46: Relative (left) and absolute (right) CSEM anomaly for 1 Ω.m box of variable width x 100m height embedded in a 100 Ω.m medium and located underneath a CSEM receiver 8km away from the CSEM source transmitting a signal at 16s (0.0625Hz).

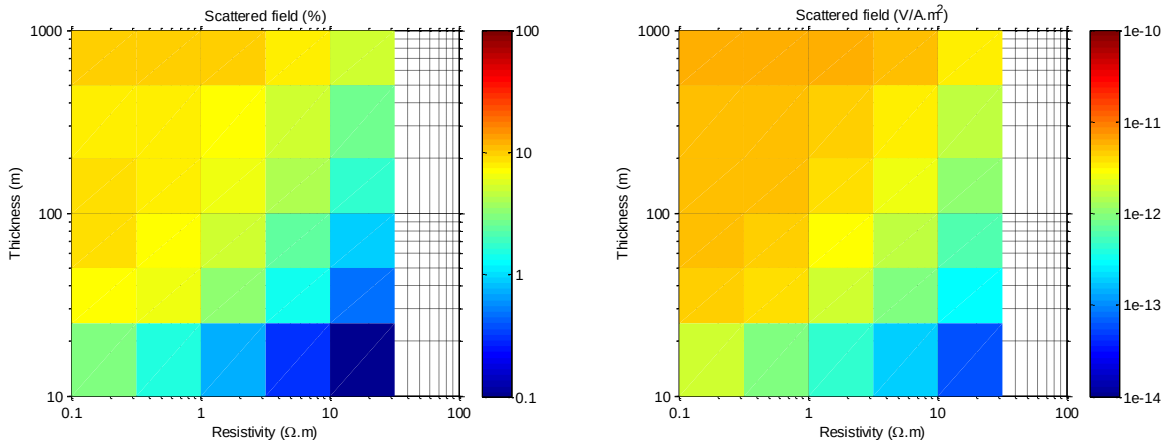

Figure 47: Relative (left) and absolute (right) CSEM anomaly for a 100m x 100m wide box of variable resistivity and height embedded in a 100 Ω.m medium and located underneath a CSEM receiver 8km away from the CSEM source transmitting a signal at 16s (0.0625Hz).

4.3.3.4 Limitations

One of the main limitations of the CSEM technique is related to the diffusive nature of the EM waves. Indeed, as shown in the previous section, it struggles to detect small bodies at great depth due to the strong attenuation of the EM waves but also to differentiate between a heterogeneous medium and its up-scaled equivalent (e.g. objects of similar transverse resistance).

Although the CSEM technique uses highly-powered electric current generator, EM noise in industrialized areas can still be stronger than the CSEM signals at the source-receiver offset of interest for geothermal exploration. On the other hand, the need of long (kilometres) electric dipoles and transmission times (hours) to stack-out ambient EM noise limits the number of transmitter/receiver positions during a CSEM survey and therefore limits the spatial coverage and hence resolution of the CSEM surveys.

4.4 Gravity

4.4.1 Principle

The gravity method studies anomalies of the earth's gravitational field that are caused by underground density variations. The Bouguer model is usually used for presenting gravity data after correction for elevation, latitude, relief and tidal effects. Bouguer anomalies are thus expected to correspond to underground geological formations or structures that have significant density contrast with their environment.

4.4.2 Benefits

Varying gravity anomalies can be associated with a geothermal system and be the target of gravity surveys. In general, gravity highs are observed as a result of mineral precipitation and/or local fracturing/alteration and late-stage leaching. Gravity lows are usually observed over sedimentary basins as a result of the lower density sediments compared to the basement and can help defining the shape and thickness of the basins.

4.4.3 Resolution

As the wavelength of the gravity anomalies depends on the depth and size of the density anomalies, the spatial resolution of the gravity method does too. To illustrate this aspect, we computed the gravity anomaly at surface generated by two 1m wide sphere separated by 1000m as a function of the horizontal position of the gravity measurement (X-axis) and depth of the spheres (Y-axis). It clearly shows at shallow depth (<1000m), the two spheres can be easily distinguished while at greater depth, the anomalies are interfering and it is no longer possible to distinguish the two objects. In the case of deep geothermal exploration, this technique will therefore be best suited to characterize large scale variations (kilometer scale), for instance at basin scale.

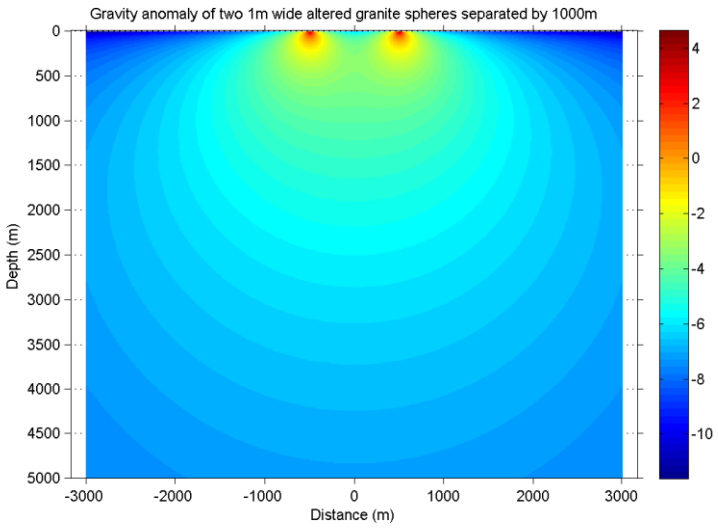

Figure 48: Gravity anomaly in m/s2 at surface generated by two 1m wide sphere separated by 1000m as a function of the horizontal position of the gravity measurement (X-axis) and depth of the spheres (Y-axis).

4.4.4 Limitations

The main limitation of this technique comes from the limited spatial resolution (previous section) and the non-uniqueness of the inversion results. Calibration data (density values from boreholes or analogues) and integration with other geophysical techniques are often required in order to reduce the size of the possible model space.

4.5 Magnetism

4.5.1 Principle

The magnetic method aims at measuring the anomalies of the earth's magnetic field caused by variations in the intensity of magnetization of rock formations and structures. Measurements can be made on the earth's surface, at a certain height using airborne systems.

4.5.2 Benefits

The magnetization of rocks is partly due to induction by the magnetizing force associated to the Earth's magnetic field and partly to their remnant magnetization. For geothermal applications, the following phenomena can produce magnetic anomalies:

- High magnetic susceptibility of the rocks (mainly basic rocks) due to their high content of magnetic minerals and particularly of magnetite
- Remnant magnetization acquired during the cooling of the igneous rocks (below the Curie temperature)
- Chemical processes altering magnetite into pyrite or hematite as a results of the action of hydrothermal fluids causing demagnetization of the rocks

4.5.3 Resolution

Magnetic surveys have similar spatial resolutions as gravity surveys (as the magnetic anomaly is the derivative of the gravity anomaly in the direction of magnetization or Poisson's relationship). As shown on Figure 48, this technique will therefore be best suited to characterize large scale variations (kilometer scale) in the case of deep geothermal exploration.

4.5.4 Limitations

The main limitation of this technique comes from the limited spatial resolution and the non-uniqueness of the inversion results. Calibration data (magnetization values from boreholes or analogues) and integration with other geophysical techniques are often required in order to reduce the size of the possible model space.

5 Geological data

5.1 Structural analysis

As the main key situations have been linked to faults and fractures, the main geological description will be dedicated to these structures at different scales. These structures are the basis of the stress and hydraulic models.

At regional scale, the large faults are called cartographical structures. They are identified on geological maps or on seismic lines in depth to constitute 3D geological model.

A more local scale, especially on analogue outcrops, fracturation is analyzed in order to bring geometrical and mechanical properties to discrete modelling (IMAGE report D7.5). Fracture data acquisitions are dedicated to:

- Orientations
- Length
- Spacing
- Termination
- Curvature
- Roughness
- Infill

From boreholes, structural data can provide from cores or image logs. Cores allow to measure orientations, if cores are oriented by correlation with image logs for example, linear spacing, roughness and infill. However, other measurements as length, termination, curvature are not available from boreholes.
On image logs, orientation and spacing have available. However, only about 20% of fractures observed on cores are visible on image logs. Roughness and nature of infill cannot be determined. Some indications of alteration can be subtracted from images and well logs like spectral gamma ray.

5.2 Petrography, mineralogy

Studies of petrography and mineralogy allow to determine the rock nature and the fracture infill. The mineralogy characterization is based on:

- first, optical microscope, in order to carry out a primary mineralogiqcal determination and a texture characterization;
- scanning electron microscope, in order to determine precisely the nature of minerals;
- cathodoluminescence, in order to discriminate the different phases of carbonate precipitation from different fluid pulses;
- electron microprobe, in order to analyze major chemical elements of carbonates and sulfates.

These analyses can be completed can be completed by microthermometric measurements, in order to determine the salinity of trapped fluids and the temperature at which the fluid has been trapped, and the isotopic analyses, in order to discriminate the origin of the fluid.

Mineralogical studies allow to reconstruct the paleocirculation in relation to tectonic history in order to determine the main fracture sets which are the best fluid pathway in the upper crust. The fluid pathways are the target for geothermal exploration in the deep sedimentary basin.

Mineralogical texture can help to understand the porosity and how the porosity pattern arranges.
And finally, the chemical characterization of fracture infill could help to determine the best chemical stimulation applied in order to enhance the fracture permeability.

6 Geochemistry

6.1 Fluid geochemical analysis

Determining the fluid compositions provide evidence of origin of the fluid: surface, basin, deep hot fluids or mixed processes. Associated with the geological knowledge, large circulation of the fluid could be proposed and give important information for hydraulic models.

6.1 Geothermometers

Isotopic analyses of the fluid give indication of the maximum equilibrium temperature. Different type of couple of chemical elements, such as Na-K, Na-K-Ca, Na-K-Ca-Mg, K-Mg, SiO_2, $\delta^{18}O_{H2O-SO4}$, are commonly used (see IMAGE report D7.3) to determine the temperature.

Associated to geochemical analyses and other regional knowledge, the data provide information of the fluid circulation within the upper crust.

6.2 Tracer tests

Tracer testing is an efficient method to detect and characterize hydraulic connections between deep geothermal wells, to understand the migration of injected and natural fluids, and to estimate their proportions in discharged fluids, their velocities, flow rates, residence times.

The tracer tests can provide information on transport properties and hydraulic connections essential for heat exchange or for fluid re-injection in geothermal reservoirs.

7 Types and scales of (T)HM models

In the framework of the improvement of exploration methods, the numerical modeling of physical processes provides useful tools in order to more accurately locate the geothermal resources in terms of heat, flow, depth *etc*. Indeed, the understanding of physical processes in a specific geodynamic system, such as fluid flow, heat transport and tectonic stresses distribution, as well as their interactions, is fundamental in order to predict the location of favourable conditions and, moreover, to explain why they are favourable. To do that, the numerical models deal with description of the geodynamic context at different scales, from the regional scale to the more local scale. At these scales, the geological structures to integrate in the model are the large homogeneous lithological blocks and the main tectonics fault zones inherited from the whole tectonic history. Depending on the modeling approach, the focus is made, on one hand, on the properties of the geological blocks for continuum approaches, and on the other hand, on the description of the fault network for discontinuum approaches (dealing with Discrete Fracture Networks). For both approaches, at these scales, the description of the properties of the different elements cannot be directly estimated from the measurements of the properties at the laboratory scale. Hence conceptualisation and assumptions are necessary to extrapolate the behavior of these large geological structures, whether they are fault zones or large lithological blocks. Furthermore, at these scales of modeling, a tricky issue concerns the choice of the boundary conditions for each studied physic (*e.g.*, displacement field or stresses for the modeling of stresses distribution). To conclude, another very important aspect is the validation of the numerical simulations by comparison of the obtained results with field data.

To sum up, the three mains difficulties of the numerical models at these scales which requires additional constraints from exploration methods are:

- The description of the geological structures and their properties: homogeneous lithological blocks, tectonic fault zones;
- The definition of boundary conditions;
- The validation of numerical simulations from field data.

8 Best Practices for Deep Geothermal

8.1 Matrix of Key Situations vs Geophysical Methods

European scale

		Heat Factor	Heat Factor	Heat Factor	Fluid factor	Fluid factor
Type of method	Method	Plutonic Intrusion	Thermal Blanket	Convective Heat Transfer	Single fault: jog/ramp/tip	Fault intersection
Active Seismic	2D Seismic	★★★	★★★	★★	★★	★★
Active Seismic	3D Seismic	★★★	★★★	★★	★★★	★★★
Active Seismic	VSP Seismic	★	★	★	★	★
Passive Seismic	Microseismic	★★	★★	★★	★★	★★
Passive Seismic	Noise tomography	★★★	★★★	★★	★	★
Active EM	ERT/CSEM	★★★	★★★	★★	★★	★★
Passive EM	MT	★★★	★★★	★★	★★	★★
Gravity		★★★	★★★	★★	★★	★★
Magnetism		★★★	★★★	★★	★★	★★
Structural		★★			★★	★★
Petrology/Mineralogy		★★★				
Fluid Geochemistry				★		
Geothermometers				★		
Tracers						

★★★ Strongly recommended
★★ Possible
★ Not recommended

To assess the heat factor of an exploration area at the European scale, all geophysical techniques are in principle suitable, except VSP's as the volume of investigation is limited around the borehole. Similarly, structural and petrological techniques can provide valuable information. However, it is usually difficult for all techniques to assess the presence of a convective cell (except possibly geochemical and geothermometer data). For the fluid factor/presence of a favourable fault network, 3D seismics combined with structural analysis is the best due its high spatial resolution but 2D seismic, passive seismic, active/passive EM and gravity/magnetism can also provide valuable information. Only VSP's and noise tomography (due to the low resolution) are not recommended. Similarly, petrological, geothermometers, geochemical and tracer data are not deemed favourable.

Regional scale

		Heat Factor	Heat Factor	Heat Factor	Fluid factor	Fluid factor
Type of method	Method	Plutonic Intrusion	Thermal Blanket	Convective Heat Transfer	Single fault: jog/ramp/tip	Fault intersection
Active Seismic	2D Seismic	★★★	★★★	★★	★★	★★
Active Seismic	3D Seismic	★★★	★★★	★★	★★★	★★★
Active Seismic	VSP Seismic	★★★	★★★	★★	★★	★★
Passive Seismic	Microseismic	★★	★★	★	★★	★★
Passive Seismic	Noise tomography	★★	★★	★	★	★
Active EM	ERT/CSEM	★★	★★	★	★★	★★
Passive EM	MT	★★	★★	★	★★	★★
Gravity		★★	★★	★	★★	★★
Magnetism		★★	★★	★	★★	★★
Structural		★★★	★★★		★★★	★★★
Petrology/Mineralogy		★★★	★★★			
Fluid Geochemistry				★★		
Geothermometers				★★		
Tracers						

★★★ Strongly recommended
★★ Possible
★ Not recommended

To assess the heat factor of an exploration area at the Regional scale, all geophysical techniques are in principle suitable as well as structural and petrological methods. However, it is usually difficult for all techniques to assess the presence of a convective cell, except geochemistry. For the fluid factor/presence of a favourable fault network, 3D seismics combined with structural analysis is the best due its high spatial resolution but 2D seismic, VSP's, passive seismic, active/passive EM and gravity/magnetism can also provide valuable information. Only the noise tomography technique (due to the low resolution) and petrology, geochemistry, geothermometers and tracers (due to their lack of sensitivity to the presence of fault network) are not recommended.

Local scale

		Heat Factor	Heat Factor	Heat Factor	Fluid factor	Fluid factor
Type of method	Method	Plutonic Intrusion	Thermal Blanket	Convective Heat Transfer	Single fault: jog/ramp/tip	Fault intersection
Active Seismic	2D Seismic	★★	★★	★	★	★
Active Seismic	3D Seismic	★★★	★★★	★★	★★★	★★★
Active Seismic	VSP Seismic	★★★	★★★	★★	★★★	★★★
Passive Seismic	Microseismic	★	★	★	★	★
Passive Seismic	Noise tomography	★	★	★	★	★
Active EM	ERT/CSEM	★	★	★	★	★
Passive EM	MT	★	★	★	★	★
Gravity		★	★	★	★	★
Magnetism		★	★	★	★	★
Structural		★★	★★		★★★	★★★
Petrology/Mineralogy		★★★	★★★			
Fluid Geochemistry				★★★		
Geothermometers				★★★		
Tracers				★★		

★★★ Strongly recommended
★★ Possible
★ Not recommended

To assess the heat factor of an exploration area at the Local scale, active seismic techniques (2D/3D seismic, VSP) combined with structural and petrological analysis are best suited. Passive seismic, active/passive EM and grav/mag will all struggle due to their limited spatial resolution as well as geochemistry, geothermometer and tracer methods. For the fluid factor/presence of a favourable fault network, 3D seismic and VSP's combined with structural analysis are best suited. All other techniques do not usually provide enough spatial resolution.

8.2 Exploration Workflow

8.2.1 Technical Feasibility Study

The first step while designing an exploration program consists in clearly identifying the geological uncertainties that need to be addressed in order to support the business decision(s) of the geothermal project. In the case of the deep EGS project, it is very likely that one or many of the key parameters of the key situations is too uncertain for a proper decision to be made and needs to be further de-risked (e.g. presence of a favorable fault network, temperature anomaly etc…). Once the geological uncertainties clearly spelled-out, the second step consists in translating these uncertainties into the range of possible geological scenarios (e.g. open/closed fault network, size/depth of the fault network etc...) and associate physical properties to them through a petro-physical study based on well logs and analogues (e.g. density, velocity, resistivity, magnetization etc…). The final step consists in performing a technical feasibility study based on numerical modelling and actual measurements on analogous sites to estimate the expected geophysical signal to noise ratios for each geological scenario and establish which exploration techniques can discriminate them. At this stage, the ability of the different techniques to answer the business question(s) is established but economic considerations have to be taken in account through a Value of Information study (VOI) in order to make the decision to acquire additional data or not.

8.2.2 Economic Value of Information (VOI) and Go-No Go Analysis

This step consists in establishing among the various exploration techniques that are likely to answer the business decisions, which are the ones that are likely to bring additional value to the project given their costs (financial, time, human resources etc…). There are many different tools for this purpose but we propose here to use the concept of the Value Of Information study (VOI) for its simplicity and flexibility.
The basic principle of a VOI study is to assess how the investment in a exploration technique is going to influence the economic value of the geothermal project. To quantify the economic value of the project, we use of the concept of Net Present Value (NPV) i.e. the expected income minus the CAPital and OPerational EXpenditures (CAPEX and OPEX) over the lifetime of the project. As projects usually carry a wide range of possible outcomes (e.g. success/failure cases), the NPV of each scenario needs to be calculated and weighted according to its probability (risked NPV = probability x NPV). Based on this economic analysis, a decision tree can be built where the decision is whether or not to acquire additional data and the values of each branch are the risked NPVs (Figure 49). A key parameter in such a tree is the degree of confidence in the exploration technique i.e. the probability of the project to succeed/fail with/without the additional piece of information (X and Y). This must be based on the technical feasibility study aforementioned and previous experiences with the technique. Another key parameter in the tree is the cost of the technique itself. As this is project depend, we propose to perform a sensitivity study of the decision and economic value of the project as a function of the cost of the data. For illustration purposes, a sensitivity study based on hypothetical project costs has been performed (Figure 50). When positive, it makes economic sense to invest in acquiring the data. When negative, the acquisition of additional data is detrimental to the project economics. The turn-over point represents the maximum cost at which the additional data must be acquired. At this point, the technical and economical elements of the VOI study can be brought together with the commercial, organizational and political elements of the decision to perform a go-no go analysis and provide recommendations on whether or not to acquire additional data in the exploration program.

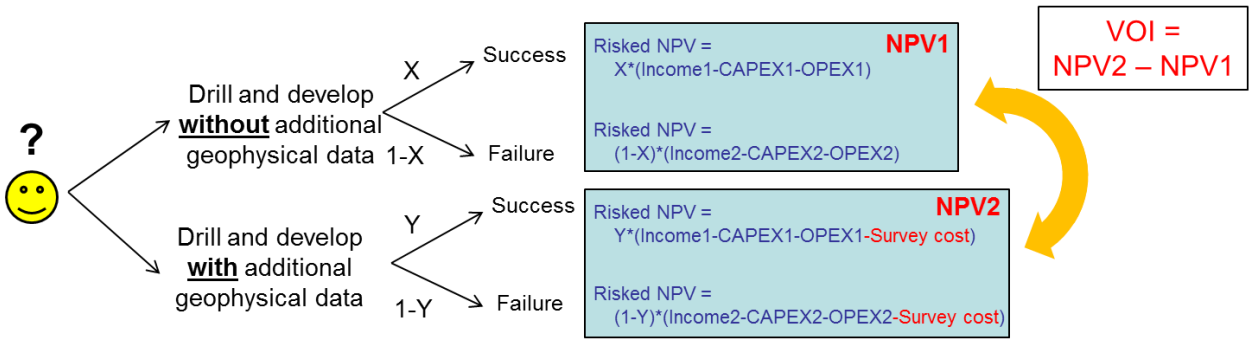

Figure 49: Decision tree on whether or not to acquire additional data to the geothermal project and definition of its VOI.

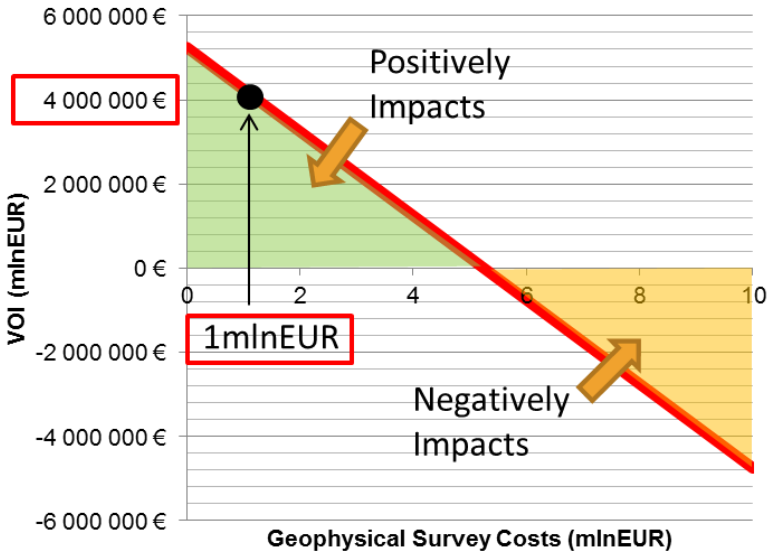

Figure 50: Example of sensitivity study of the decision and economic value of the project as a function of the cost of the exploration method. When positive, it makes economic sense to invest in acquiring the data. When negative, the acquisition of additional data is detrimental to the project economics. The turn-over point represents the maximum cost at which the additional data must be acquired.

8.2.3 Data Acquisition

This step consists in gathering, processing the data that is required to discriminate the various geological scenarios described in section 8.2.1. It is important to keep this objective in mind throughout the process in order to keep the right balance between data quality and cost. Typical survey size, duration and costs for the different geophysical techniques of interest for geothermal exploration are shown on Figure 51, highlighting the tradeoffs between data types, costs and delivery time.

	Equipment	Spatial Resolution	Crew size	Typical Price Tag	Typical Survey Duration	Typical Processing/ Imaging Duration	Peri-Urban Areas
Active Seismic	Vibroseis + 1C/3C geophones	10's m	10's people	100's k€/km2 (3D) 10's k€/km (2D)	Weeks	Months	Challenging
Passive Seismic	Natural acoustic emissions + Seismometers	100's m	A few people	A few k€/km2	Months	Weeks	Acceptable
Active EM (CSEM)	Electric dipole + MT stations	100's m	A few people	10's k€/km2	Weeks	Months	Challenging
Passive EM (MT)	Natural EM waves + MT stations	100's m	A few people	A few k€/km2	Weeks	Weeks	No-Go
Gravity/ Magnetics	Land/airborne sensors	1000's m	A few people	A few k€/km2	Weeks	Days	Acceptable

Figure 51: Typical survey size, duration and costs for different geophysical techniques of interest for geothermal exploration.

8.2.4 Data integration and Decision Making

This step is the last but not the least of the exploration workflow. It consists in putting the newly acquired data back into the geological context for proper business decision making. This integration step is very important to establish how these data are discriminating the different geological scenarios of interest. It is also important to realize that some scenarios may not be discriminated based on single (e.g. geophysical or geological) data only but rather on the combination of these (Figure 52).

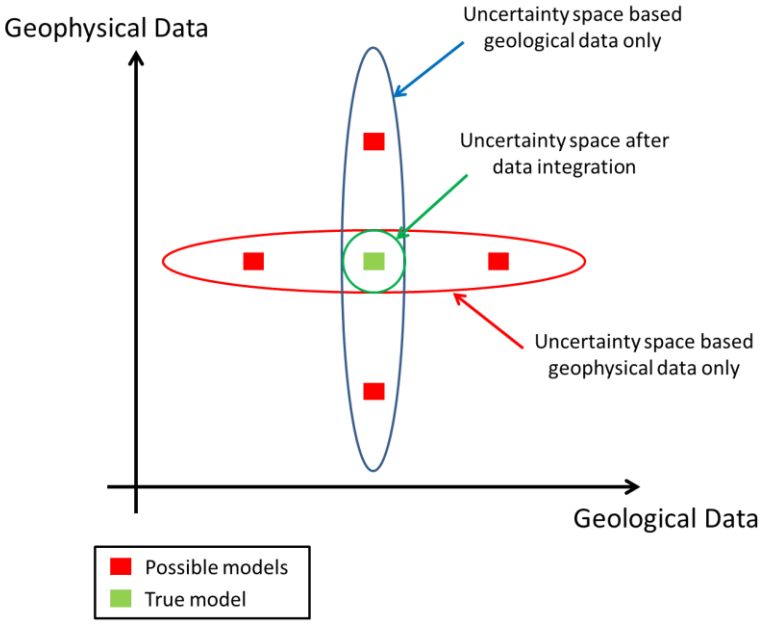

Figure 52: Uncertainty space based on geological (blue) and geophysical (red) data only and the integration of all data (green). Possible models are shown in red and the true model in green.

9 Conclusions

The selection of the exploration techniques and types of subsurface models that can be derived from them is very dependent on the scale of the exploration program (Figure 53). There are therefore no golden rules to select the best exploration techniques for a given geothermal project in a sedimentary basin but rather a wealth of techniques that must be tailored based on their technical feasibility, spatial resolution, delivery time and costs. This report aims at giving some guidance on the selection but discipline experts must always be consulted prior to embarking into an exploration program.

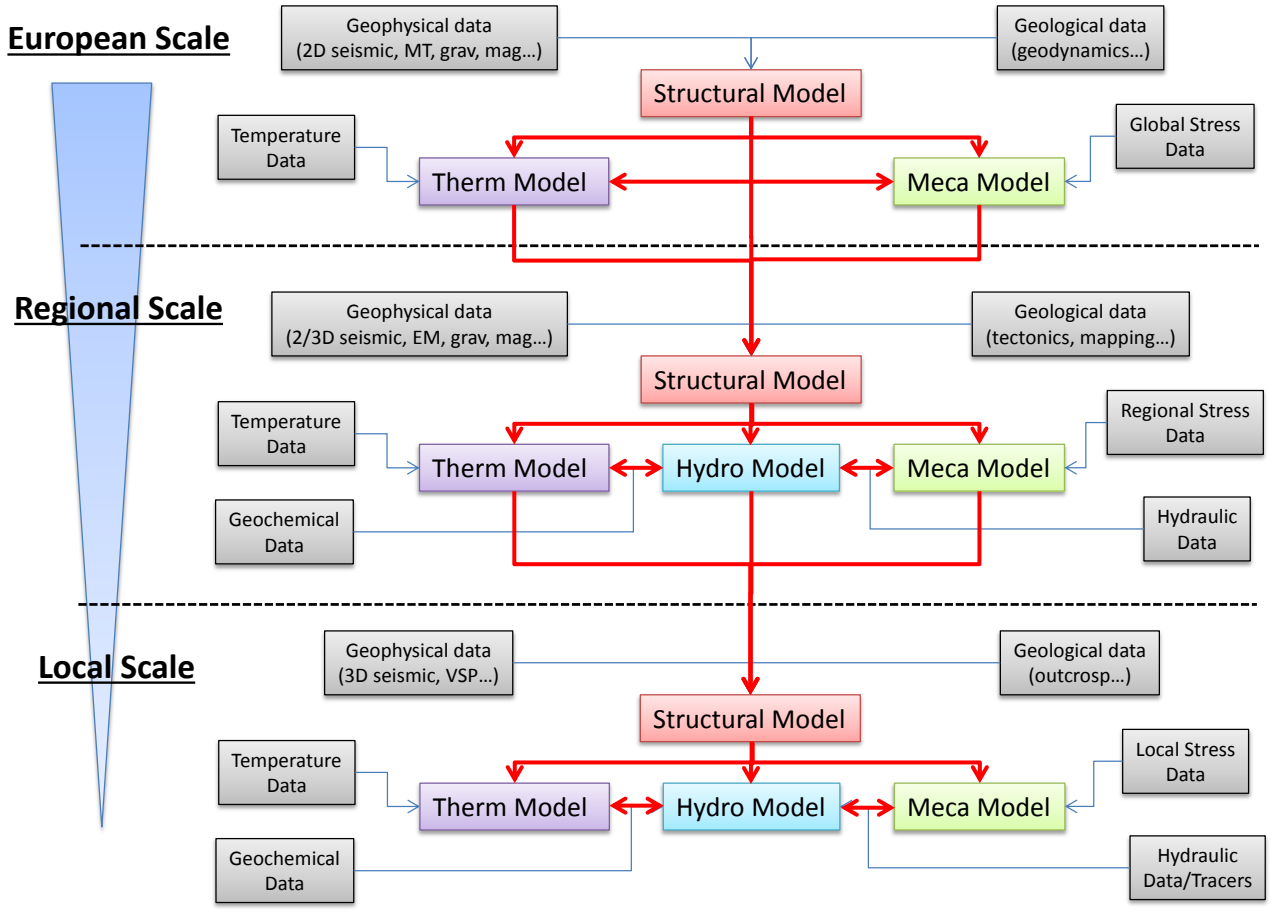

Figure 53: Exploration techniques and type of subsurface models that can be derived from them as a function of the exploration scale.

10 Bibliography

Aki, K. (1957), Space and time spectra of stationary waves with special reference to microtremors, Bull. Earthquake Res. Inst. Univ. Tokyo, 35, 415–456.

Batzle, M. and Wang, Z., 1992, Seismic properties of pore fluids: Geophysics, Vol. 57, No. 11, p. 1396-1408.

Bense V.F., Gleeson T., Loveless S.E., Bour O., Scibek J., 2013, Fault zone hydrogeology, Earth-Science Reviews 127, pp. 171–192

Brune, J. N. (1970), Tectonic stress and the spectra of seismic shear waves from earthquakes, J. Geophys. Res., 75(26), 4997–5009, doi:10.1029/JB075i026p04997.

Cacace , 2010, Cacace, M., B. O. Kaiser, B. Lewerenz, and M. Scheck-Wenderoth (2010), Geothermal energy in sedimentary basins: What we can learn from regional numerical models, Chem. Erde, 70(3), 33–46, doi:10.1016/j.chemer.2010.05.017.

Caine , 1996 - Caine JS, Evans JP, Forster CB (1996) Fault zone architecture and permeability structure. Geology 24(11):1025–1028. doi:10.1130/ 0091-7613(1996)024h1025:FZAAPSi2.3.CO;2,

Castera J., Dezayes C., Calcagno P., 2008, Large scale 3D geological model of the Soultz site. EHDRA meeing, Soultz-sous-Forêts.

Connolly P. T. & Cosgrove J. W., 1999, Prediction of static and dynamic fluid pathways within and around dilational jogs, In: Mccaffrey, K. J. W., Lonergan, L. & Wilkinson, J. J. (eds) Fractures, Fluid Flow and Mineralization. Geological Society, London, Special Publications, 155, pp. 105-121.

Cox S.F. & Ruming K., 2004, The St Ives mesothermal gold system, Western Australia—a case of golden aftershocks?, Journal of Structural Geology 26, pp. 1109–1125

Dezayes C., Beccaletto L., Oliviero G., Baillieux P., Capar L., Schill E., 2011, 3-D cisualization of a fractured geothermal field : the example of the EGS Soultz site (northern Upper Rhine Graben, France). Thirty-Sixth Workshop on Geothermal Reservoir Engineering, Stanford University, Stanford, California, January 31 - February 2, 2011.

Faulds, J.E., Coolbaugh, M.F., Hinz, N.H., Cashman, P.H.,and Kratt, C., Dering, G., Edwards, J., Mayhew, B., and McLachlan, H., 2011, Assessment of favorable structural settings of geothermal systems in the Great Basin, western USA: Geothermal Resources Council Transactions, v. 35, pp. 777-784. (2011)

Faulkner D.R., Jackson C.A.L., Lunn R.J., Schlische R.W., Shipton Z.K., Wibberle C.A.J., Withjack M.O., 2010, A review of recent developments concerning the structure, mechanics and fluid properties of fault zones. J. of Structural Geol., 32, 1557-1575.

Ferril D.A.& Morris A.P. , 2001, Displacement gradient and deformation in normal fault systems, Journal of Structural Geology 23 (2001) pp. 619-638

Freymark, J., Sippel, J., Scheck-Wenderoth, M., Bär, K., Stiller, M., Kracht, M., and Fritsche, J.-G., 2015, Heterogeneous crystalline crust controls the shallow thermal field – a case study of Hessen (Germany) Energy Procedia, v. 76, p. 331-340.

Genter A., Traineau H., Ledésert B., Bourgine B., Gentier S., 2000, Over 10 years of geological investiguations within the HDR Soultz project, France. Proceeding World Geological Congress, Kyushu-Tohoku, Japan, May 28, -June 10, 2000.

Genter.A., Traineau H., Artignan D., 1997, Synthesis of geological and geophysical data at Soultz-sous-Forêts (France)., BRGM/RR-39440-FR

Greenhalgh S.A., Reiser F., Girard J.F., Bretaudeau F., Capar L. And Bitri A., 2015, New active seismic processing techniques developed, Milestone Report 7.1.

Limbergen J., van Wees J.-D., Tesauro M., Bonté D., Lipsey L., Beekman F., Cloetingh S., 2015, Thermo-mechanical model of the European lithosphere. Mid-term IMAGE conference, Pisa 12:13 october 2015.

Loke, M.H. and Barker, R.D. (1996), Practical techniques for 3D resistivity surveys and data inversion1. Geophysical Prospecting, 44: 499–523. doi:10.1111/j.1365-2478.1996.tb00162.x

Lüschen, E., Wolfgramm, M., Fritzer, T., Dussel, M., Thomas, R., & Schulz, R. (2014). 3D seismic survey explores geothermal targets for reservoir characterization at Unterhaching, Munich, Germany. Geothermics, 50, 167-179.

Micarelli L. & Benedicto A., 2008, Normal fault terminations in limestones from the SE-Basin (France): implications for fluid flow - From: WIBBERLEY, C. A. J., KURZ, W., IMBER, J., HOLDSWORTH, R. E. & COLLETTINI, C. (eds) The Internal Structure of Fault Zones: Implications for Mechanical and Fluid-Flow Properties. 299, DOI: 10.1144/SP299.8, pp. 123–138.

Peter M., Dezayes C., Siaut J., Valley B., 2016, Analogue field work. IMAGE report D7.05.

Place, J., Diraison, M., Naville, C., Géraud, Y., Schaming, M., & Dezayes, C. (2010). Decoupling of deformation in the Upper Rhine Graben sediments. Seismic reflection and diffraction on 3-component Vertical Seismic Profiling (Soultz-sous-Forêts area). Comptes Rendus Geoscience, 342(7), 575-586.

Place, J., Sausse, J., Marthelot, J. M., Diraison, M., Géraud, Y., & Naville, C. (2011). 3-D mapping of permeable structures affecting a deep granite basement using isotropic 3C VSP data. Geophysical Journal International, 186(1), 245-263.

Revil, A. and Glover, P.W.J. (1998). Nature of surface electrical conductivity in natural sands, sandstones, and clays. Geophysical Research Letters 25: doi: 10.1029/98GL00296. issn: 0094-8276.

Richardson S. W. & Oxburgh E. R., 1979, The heat flow field in mainland UK, Nature 282, 565 - 567 (06 December 1979); doi:10.1038/282565a0

Roux, P., K. G. Sabra, P. Gerstoft, W. A. Kuperman, and M. C. Fehler (2005), P-waves from cross-correlation of seismic noise, Geophys. Res. Lett., 32, L19303, doi:10.1029/2005GL023803.

Rowland, J.V.,& Sibson, R.H., 2004, Structural controls on hydrothermal flow in a segmented rift system, Taupo Volcanic Zone, New Zealand: Geofluids, v. 4, p. 259−283

Sanjuan B., Gal F., Millot R., Dezayes C., Jirakova H., Frydrych V., Nawratil de Bono C., Martin F., 2016, Final report on chemical geothermometers and tracers. IMAGE report D7.08.

Sausse J., Dezayes C., Genter A. and Bisset A., 2008, Characterisation of fracture connectivity and fluid dlow pathways derived from geological interpretation and 3D modelling of the deep seated EGS reservoir od Soultz (France). Thirty-Third Workshop on Geothermal Reservoir Engineering. Stanford University, Stanford, California, January 28-30, 2008.

Schmelzbach C., Carpentier S., Reiser F., Steeghs P., Maurer H., Greenhalgh S., 2016, Active seismic at basement and sedimentary. IMAGE Report D7.1.

Shapiro and Campillo, 2004, Emergence of broadband Rayleigh waves from correlations of the ambient seismic noise, GEOPHYSICAL RESEARCH LETTERS, VOL. 31, L07614, doi:10.1029/2004GL019491

Sibson, R.H. 2000. Fluid involvement in normal faulting. J. Geodynamics 29, 469-499.

Spencer, J.W. and Nur, A. (1976). “The effect of pressure, temperature and pore water on velocities in Westerly granite”, J. Geophys. Res., 81, pp. 899–904.

Szalaiova E., Iwanowski-Strahser K. and Rabbel W., 2015, 3D fracture networks in the crystalline upper crust - A new seismic model of the Continental Deep Drilling Site (South Germany), Geophysical Prospecting, 2015, 63, 937–956 doi: 10.1111/1365-2478.12268

Theissen and Rüpke, 2010, Feedbacks of sedimentation on crustal heat flow: Newinsights from the VØring Basin, Norwegian Sea, Basin Research (2010) 22, doi: 10.1111/j.1365-2117.2009.00437.x, pp. 976–990

van Wees, J.D., van Bergen, F., David, P., Nepveu, M., Beekman, F., Cloetingh, S., 2009, Probabilistic tectonic heat flow modelling for basin maturation: assessment method and applications, Marine and Petroleum Geology 26 (4),doi:10.1016/j.marpetgeo.2009.01.020, pp. 536-551

Waldhauser F. and W.L. Ellsworth, 2000, A double-difference earthquake location algorithm: Method and application to the northern Hayward fault, Bull. Seism. Soc. Am., 90, 1353-1368.

Zhang X., Jeffrey R.G. and Wu B., 2015, Coupling of rupture growth and fluid flow along a shear fracture containing structural complexities

Zhang, X., Jeffrey, R.G., Thiercelin, M., 2007. Deflection and propagation of fluid- driven fractures at frictional bedding interfaces: a numerical investigation. J. Struct. Geol. 29, 396–410.